Steel Structures Under Cyclic Unequal Deflections

Structures en acier soumises à des déflexions cycliques inégales

Stahlkonstruktionen unter zyklischer nicht konstanter Deformation

M. M. GHAMIAN
Research Student, Department of Civil Engineering, University of Waterloo, Waterloo, Ontario, Canada

S. KRISHNASAMY
Research Engineer, Ontario Hydro Research Division, Toronto, Ontario, Canada (associated with the University of Waterloo during this investigation)

A. N. SHERBOURNE
Professor of Civil Engineering and Dean of Faculty of Engineering, University of Waterloo, Waterloo, Ontario, Canada

Abstract

The behaviour of cantilever beams under the constraint of symmetrical and unsymmetrical cyclic deflections is investigated theoretically as well as experimentally. An analytical technique is developed to predict the behaviour of cantilever beams from cyclic moment-curvature relations derived from cyclic strain control tests. Twenty tests were conducted on rectangular structural steel sections under pure bending to establish these relations which couple the moment range and mean moment to curvature range. A linear nonlinear model is proposed which fits the moment range data; a tripartite model is suggested to fit the mean moment data. The models are capable of accommodating, in discrete form, the phenomena of hardening and softening of aggregation of fibers constituting a structural section as well as relaxation of the mean moment.

Nine tests were conducted on cantilever beams under completely and partially reversed tip deflections. The load range changed little with changes in mean deflection. The mean load, in general, relaxed with increasing cycling. The theory presented modelled the experimental behaviour fairly accurately. It also suggested that the behaviour may be comprised of

1. an elastic case, where mean load is proportional to load range,
2. an intermediate range where the effects of mean deflection cannot be ignored, and

3. the case of large inelastic cyclic deformation where the effects of mean deflection can be completely ignored except for associated changes in structural geometry and its secondary membrane effects.

Introduction

Cyclic loads have long been recognized as a cause of failure in structural elements such as aircraft components, pressure vessels, turbines, etc. These loads usually produce nominal (global) elastic stresses and highly localized plastic flow leading to conventional fatigue failure. Despite the fact that this topic has been the subject of extensive study, the phenomenon of fatigue is not yet fully understood from the engineering point of view. Low-cycle fatigue, on the other hand, deals with failure of components where the stress is in excess of the yield stress and the number of cycles necessary to promote failure ranges from one quarter of a cycle (monotonic failure) to 10^5. Failure at 10^6 cycles or more is considered to be the domain of conventional or high-cycle fatigue.

Most of the early work involving repeated loads on structures above the elastic limit concerned the shakedown problem. NEAL [1] proved that a structure can accumulate increasing deflections under a particular load cycle such that the structure becomes unserviceable. This kind of failure was designated "incremental collapse". Various experiments [2, 3] were conducted to establish the shakedown load leading to the proposition that theoretical predictions of shakedown loads are, in general, conservative. The main reason for such divergence between theory and experiment is that section behaviour is assumed to be invariant (elastic-plastic or static strain-hardening) regardless of cyclic history.

An altogether different approach to the same problem includes provision for the change in material response to cyclic loads and consideration of the highly non-linear nature of the problem.

The nature of the cyclic loading on structures is random, and consequently it is very difficult to study such a complex problem directly. The loading conditions can be divided simplistically into load and deformation control. At the structural, sectional and fiber level this corresponds respectively to load, moment and stress on the one hand, and deflection, curvature and elongation on the other.

ROYLES [4] suggested a moment-curvature relation derived from stable sectional behaviour under deformation control conditions. He predicted the behaviour of single and three-span continuous beams under completely reversed deflections, each subjected to a single concentrated load at the central section. Experiments were conducted on similar structures and the results were compared with theoretical predictions.

SHERBOURNE and KRISHNASAMY [5] suggested two models for the cyclic moment-curvature relation under deformation control: one model takes into account initial linear elastic behaviour and the other ignores it. They predicted the cyclic response of a cantilever beam under a single concentrated load at its tip. The tip deflection was cycled between two fixed symmetric values. Tests were carried out on the same beam configuration and experimental results were found to be in reasonable agreement with theoretical predictions.

A major shortcoming of the method after Royles was its inability to predict the behaviour of the structure at each cycle of loading. The theory developed by Sherbourne and Krishnasamy, however, can predict the response of a structure at every stage of loading.

TOPPER [6] suggested a derivation of the cyclic moment-curvature relation (for deformation control problem) from cyclic stress-strain data and section geometry. This idea was developed by other researchers (ROYLES [4], SHERBOURNE and KRISHNASAMY [5]) and proved acceptable.

A moment-curvature model under load control was suggested by KRISHNASAMY et al. [7]. It incorporates cyclic strain accumulation effects (creep) by introducing a cyclic (or time) dependent function into the moment-curvature relation. Using this expression one can predict the behaviour of a cantilever beam under completely reversed load applied at its tip. Experiments were performed on similar structures to verify theoretical predictions.

In the load and deformation control problems discussed above, only fully reversed (or alternating) conditions were considered. But it is seldom that a structural element will be subjected to alternating loading only and, here, it is necessary to investigate situations where mean loading is present.

The present work concerns mild steel beams under deflection control where the limits of cyclic deflection need not be symmetrical about the initial rest position. Obviously, unsymmetrical deflection limits will, in general, give rise to mean load, present at all times in the system; the relaxation of this mean load is also investigated. The theory postulated herein proposes that cyclic structural behaviour can be predicted from sectional behaviour where the latter is a function of cyclic material properties and sectional geometry. Hence, relevant moment-curvature models can also be developed under these ambient conditions.

Experimental

The experimental program is divided into two parts. The first consists of experiments on pure bending specimens to establish cyclic moment-curvature relations. The second part is concerned with the testing of a set of cantilever beams subjected to cyclic unsymmetric deflections. Both the pure bending and the cantilever beam specimens were made from the same material, received the same heat treatment and were tested under similar ambient conditions.

The specimens were machined from $^3/_8 \times 1^1/_2''$ hot-rolled, semi-killed, 1020 mild steel bars, the chemical composition of which is shown below.

Si	S	P	Mn	C	Ni	Cr	Mo	V	Cu	Fe
0.210	0.025	0.010	0.710	0.203	0.063	0.050	0.010	0.003	0.16	remainder

Fig. 1 shows a monotonic stress-strain curve obtained from a typical axially loaded coupon. The experiment was conducted in an Instron Universal Testing Machine and strains were measured by a clip-on extensometer mounted on the test section of the specimen.

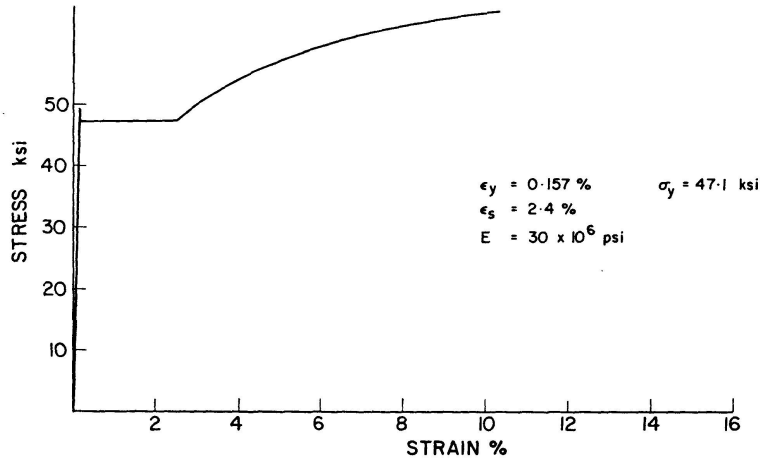

Fig. 1. Stress-Strain Curve.

All specimens were rough machined and then stress-relieved by retreating at 1600° F for a half hour and air cooling to room temperature. The final finish was carried out with care to minimize any residual stresses that might be induced.

The frequency of cycling for both kinds of tests (pure bending and cantilever) ranged between 6 and 15 cpm. Sufficient evidence is available to show that material response in this range can be considered as practically independent of frequency [8]. Moreover, the experiments were conducted under deformation control. KESHAVAN [8] showed that frequency plays a more significant role in load control than in deformation control. The wave shape used was sinusoidal throughout the experiments; the effects of wave shape are discussed elsewhere [8].

The test frame used employed a closed-loop servo-hydraulic (self-correcting) system, Fig. 2. A hydraulic actuator applied the load to the specimen and a load cell measured the load or reaction, depending upon the set-up of the testing fixture. The actuator ram displacement is measured electrically by means of a Linear Variable Differential Transformer (LVDT). Either the load or the ram displacement signal can be used as a control mechanism; thus one can obtain load or stroke control.

The pure bending device shown in Fig. 3 and used by previous researchers [9] is used in the present study. It makes use of the principle of four-point

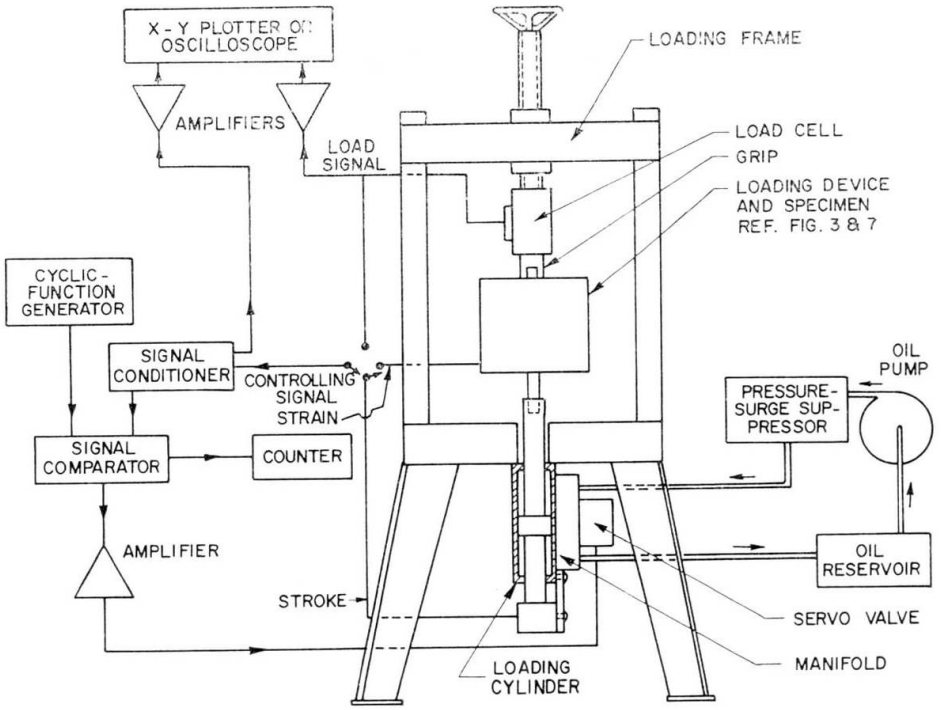

Fig. 2. Testing System.

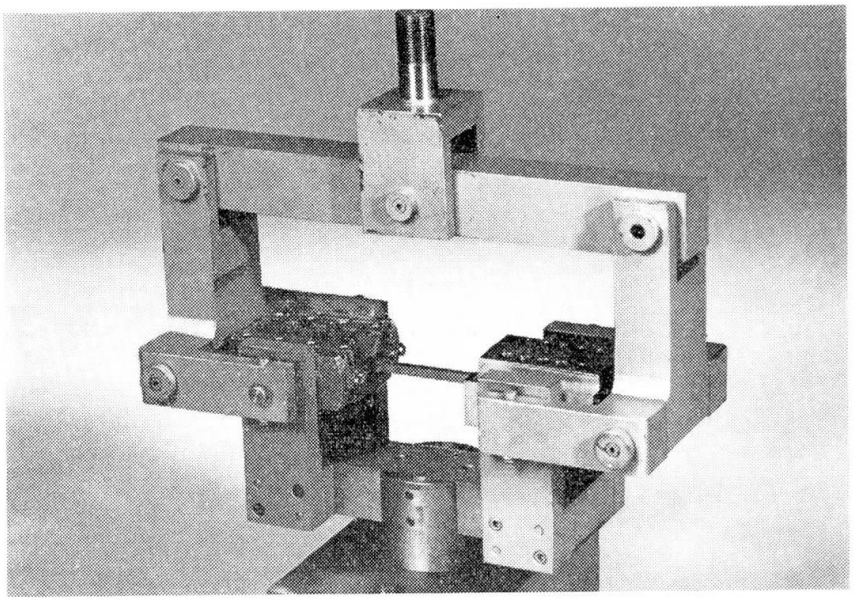

Fig. 3. Pure Bending Device.

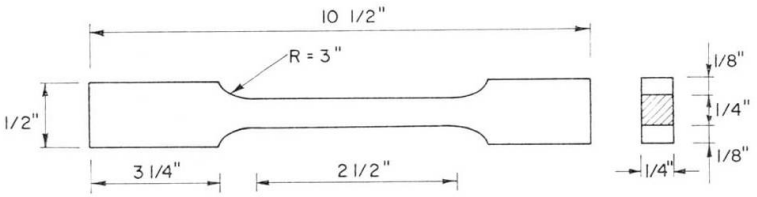

Fig. 4. Pure Bending Specimen.

loading which produces a region of uniform moment in which the bending specimen of Fig. 4 is placed. The device basically "converts the axial movement of the (test frame) ram into two equal and opposite rotations" at the ends of the bending specimen [9]. From the dimensions of the device, the uniform bending moment can be related to the load as measured by the load cell. The relation between ram displacement (stroke) and test section curvature was established experimentally as indicated in Fig. 5. The advantages of using stroke control (the case in the present work) over curvature control (measuring the extreme fiber strain by an extensometer) are indicated elsewhere [10].

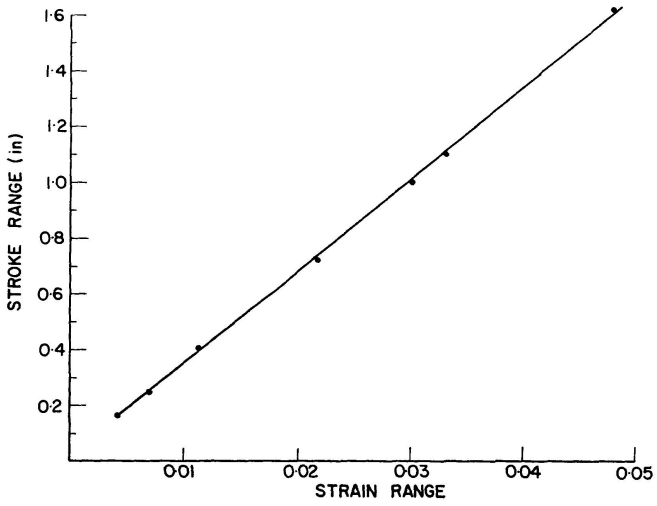

Fig. 5. Stroke Versus Strain Calibration Chart.

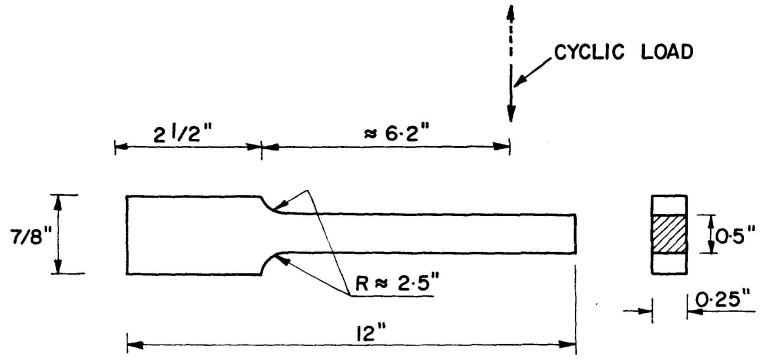

Fig. 6. Cantilever Beam Specimen.

The cantilever beam specimen is shown in Fig. 6. The depth of its haunched section is a function of the location and the two radii of fillet curvature (Appendix I). Each radius was measured accurately by means of an optical device. Simple measurements yielded the depth at consecutive sections along the beam length. The depth and width of these consecutive sections provide the input for a computer program, that will be presented later, to determine beam response.

The cantilever beam fixture shown in Fig. 7 was used previously [11] and is subject to minor modifications. The beam (1) is held at the "fixed end" by fixture (2) which, in turn, is fastened to the test frame hydraulic ram (3). The cyclic concentrated load, on the other hand, is applied to the beam at its "tip"

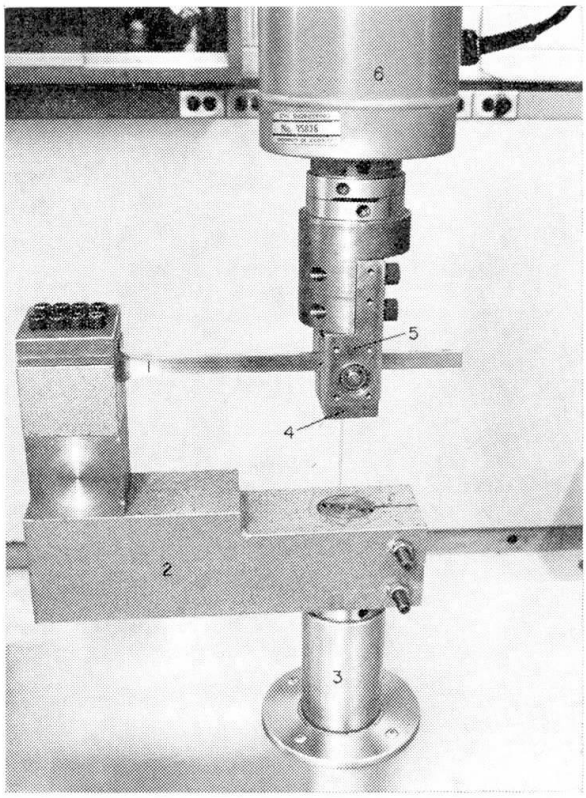

Fig. 7. Cantilever Beam Fixture.

by two rollers contained in a box (4). This box swings about an axis that connects it to a supporting element (5) attached to the load cell (6).

The load is measured by the load cell and the deflection of the beam's fixed end with respect to the free end is considered equal to the ram displacement. This implies that the test frame deformation is negligible as was verified experimentally.

Control Conditions

The trace of cyclic generalized force with respect to the corresponding generalized deformation yields a hysteresis loop that degenerates to a straight line when no plastic deformation is involved. At the sectional level this is a moment-strain loop. If the strain limits are fixed, any increase in the moment range is interpreted as hardening and any decrease as softening. Similarly, for fixed moment limits, an increase in strain range is softening; a decrease is hardening.

Other phenomena exhibited by the hysteresis loop are those of cyclic creep and relaxation. The first is an accumulation of strain (curvature) under load (moment) control; the second is a decrease in mean load (moment) under deformation (curvature) control. The pure bending tests discussed in the following section were conducted under exclusively constant strain control; hence, cyclic creep was not present.

Pure Bending

Moment Strain Relations

Fig. 8 shows the moment range versus cyclic state for a constant curvature range (or extreme fibre strain range). The moment range decreases with life, Fig. 8a. For larger strain ranges, however, the moment range remained practi-

Fig. 8a–g. Cyclic Variation of Moment Range and Mean Moment.

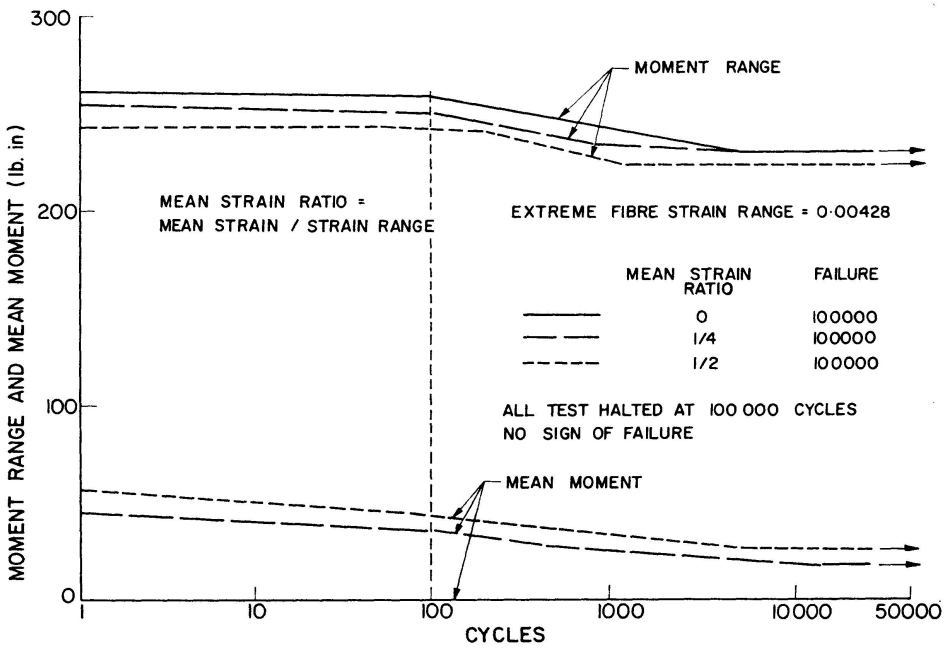

Fig. 8a.

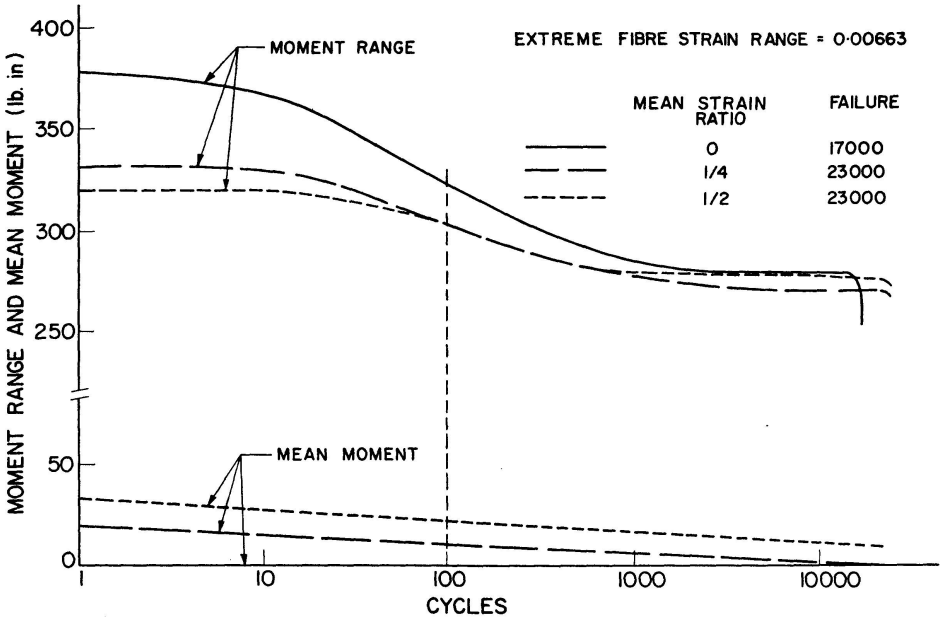

Fig. 8b.

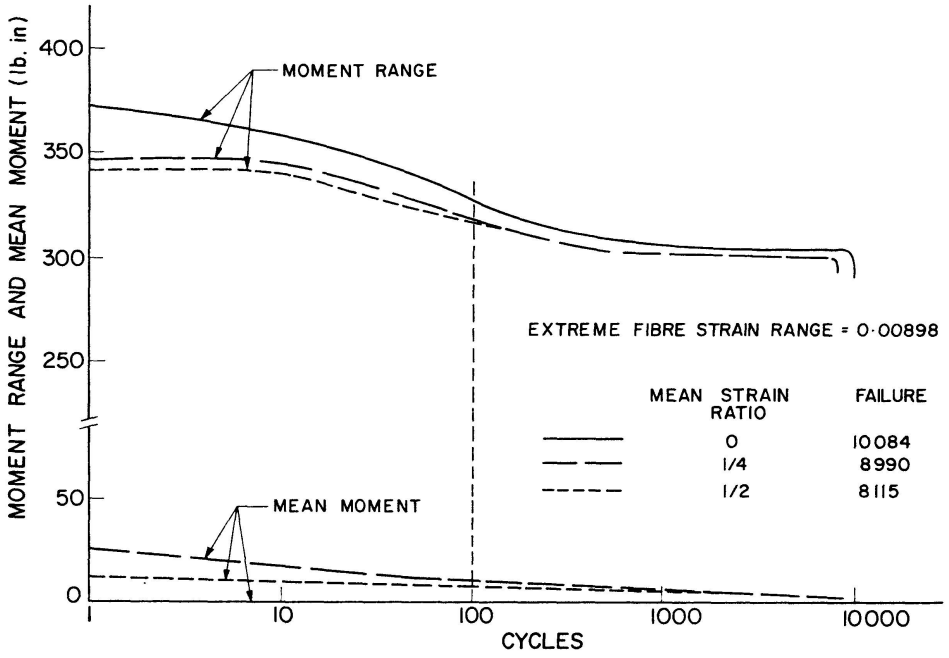

Fig. 8c.

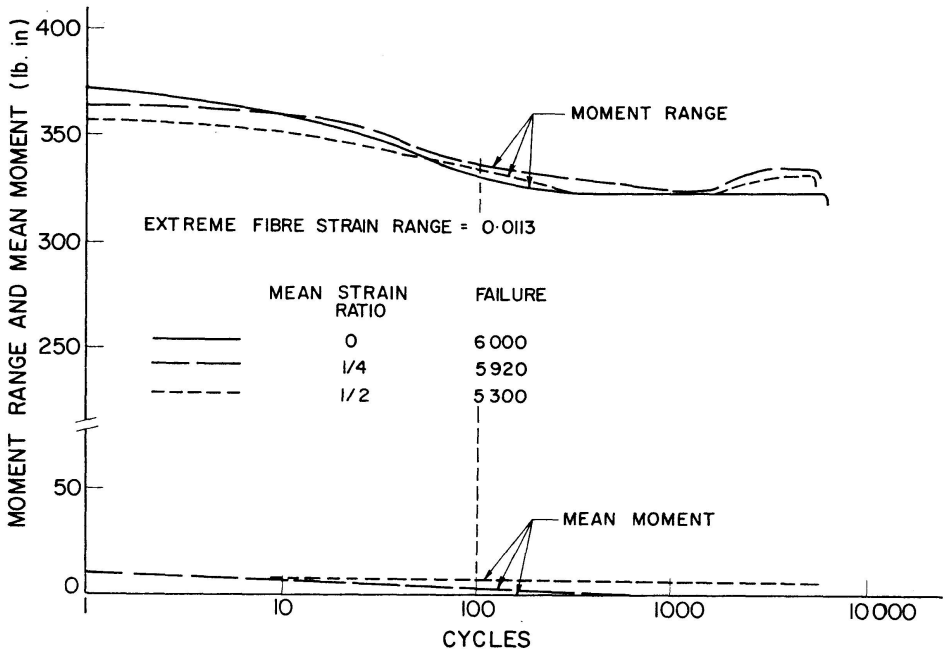

Fig. 8d.

cally constant or even increased, Figs. 8e, f, g. Hence the section as an aggregation of fibres, may be softening, stable or hardening depending upon the cyclic strain ranges involved in the individual elements.

The experimental results demonstrated that the moment range, for a certain strain range, varies little with the change in the mean strain value. Fig. 8d, for example, shows the moment range versus number of cycles for an extreme fiber strain range of 0.0113 and mean strain ratios of 0, 0.25 and 0.5. The maximum discrepency from the average value is less than 2%. For

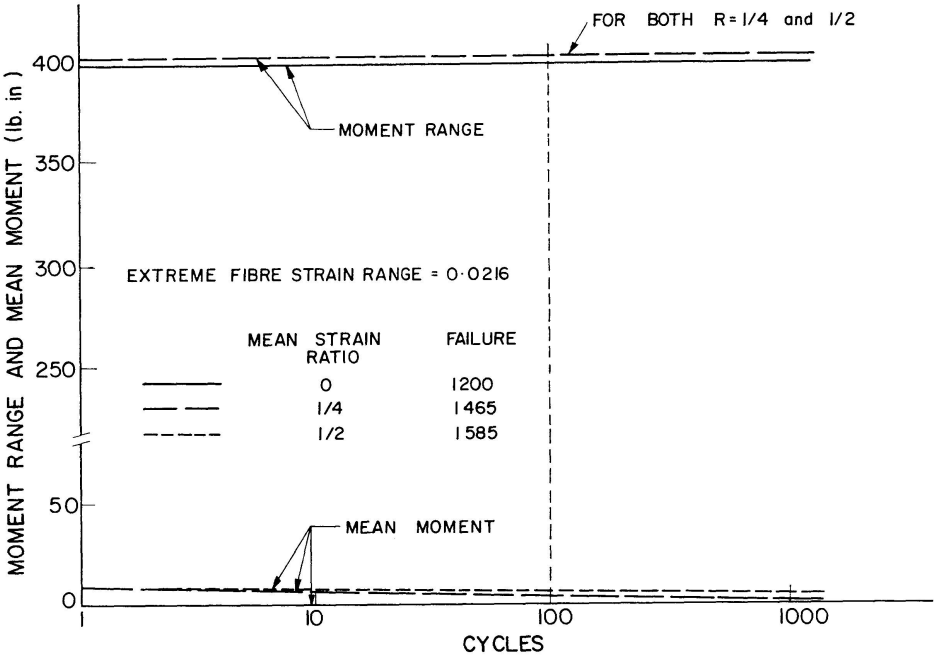

Fig. 8e.

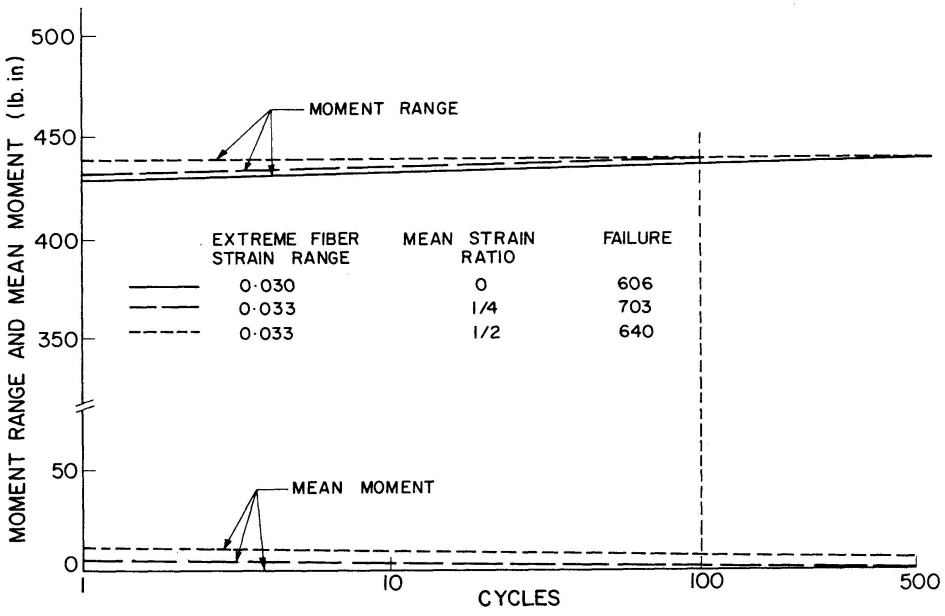

Fig. 8f.

this strain range the section softens during the initial 300 cycles or so then almost stabilizes for the remainder of its life.

The case where the mean strain has the greatest effect on moment range is depicted in Fig. 8b. This is due to the fact that the loop corresponding to zero mean strain and the given strain range has a small plastic strain component whereas that incorporating mean strain has a larger plastic component. This is illustrated in Figs. 9a and 9b. Nonetheless, for higher cycles, larger plastic strain would have developed within the total strain range of Fig. 9a, and the moment range approaches the value exhibited by the other specimens. The

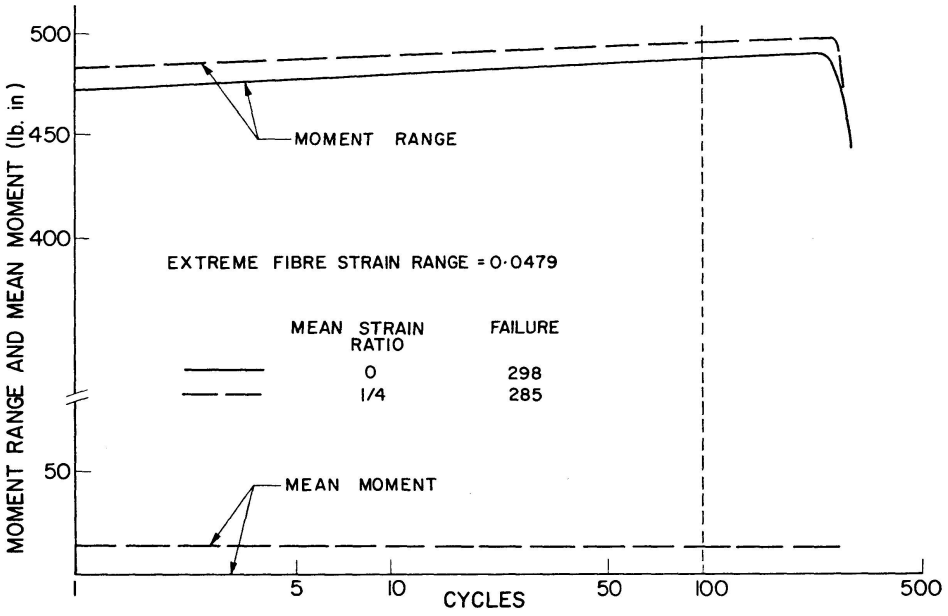

Fig. 8g.

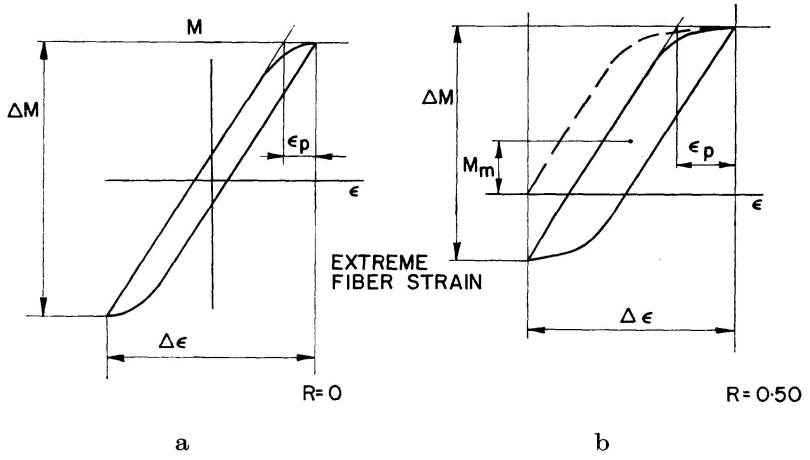

Fig. 9. Effect of Plastic Strain Component on Moment Range.

greatest discrepancy, however, is of the order of 15%. Such discrepancy will be ignored in the modelling suggested below, i.e., only an average moment range-strain range relation will be adopted for any cyclic stage regardless of the mean strain ratio. This may cause some predictive error only in the early stages of life of the structure. The significance of the error introduced will be discussed later.

The diagrams of Fig. 8, in addition to showing the moment range variation versus the number of cycles, show the relaxation of mean moment. It is clear that, for all strain ranges, the mean moment, in general, is a function of the mean strain.

Life span, on the other hand, did not seem to be significantly affected by mean strain. The tests, as a whole, did not show any definite trends in this

Fig. 10a–g. Discrete Cyclic Moment-Strain Relations.

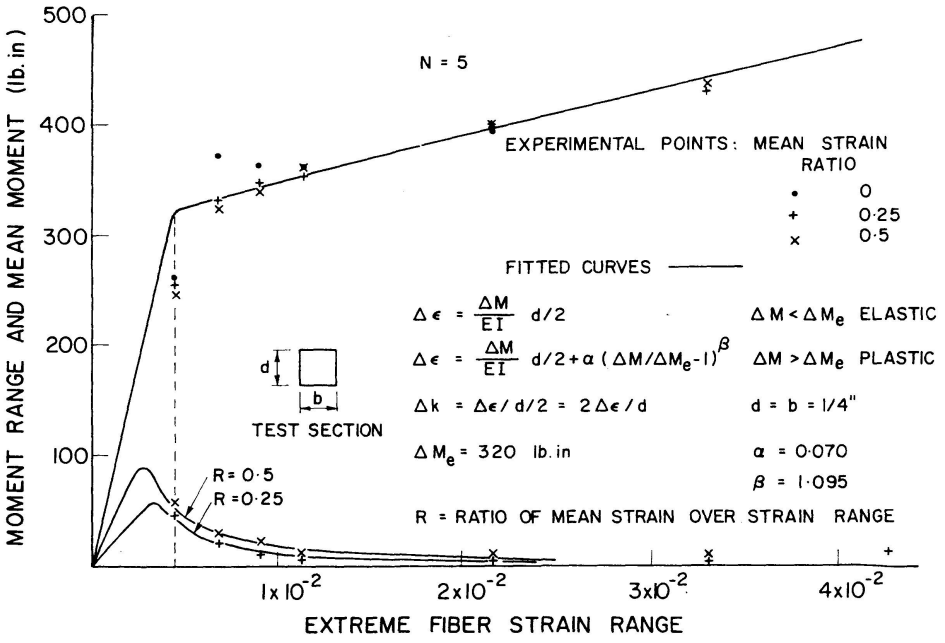

Fig. 10a.

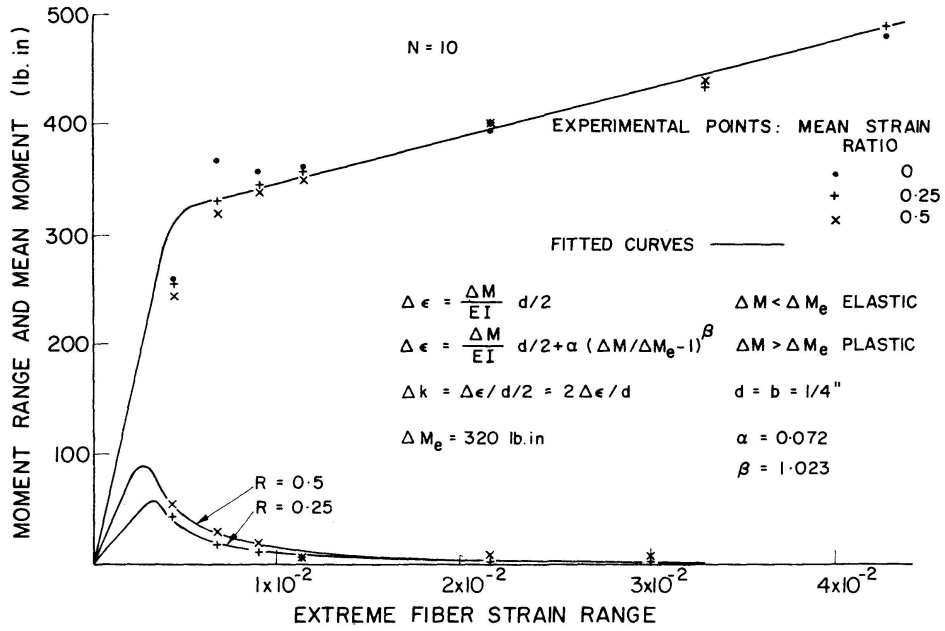

Fig. 10b.

direction and the lack of correlation can probably be accounted for by the scatter inherent in fatigue behaviour.

For a certain cyclic state, the compilation of moment range versus strain range data yields cyclic moment range-strain range relation as shown in Fig. 10. Similarly, the compilation of mean moment versus strain range yields corresponding cyclic mean moment-strain range relation. As an example, Fig. 10d

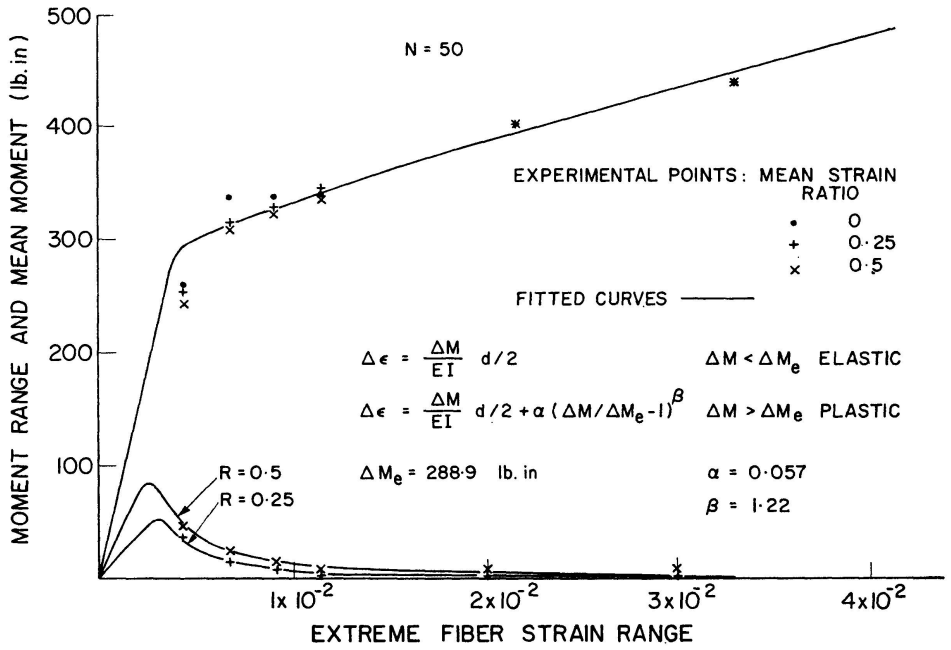

Fig. 10c,

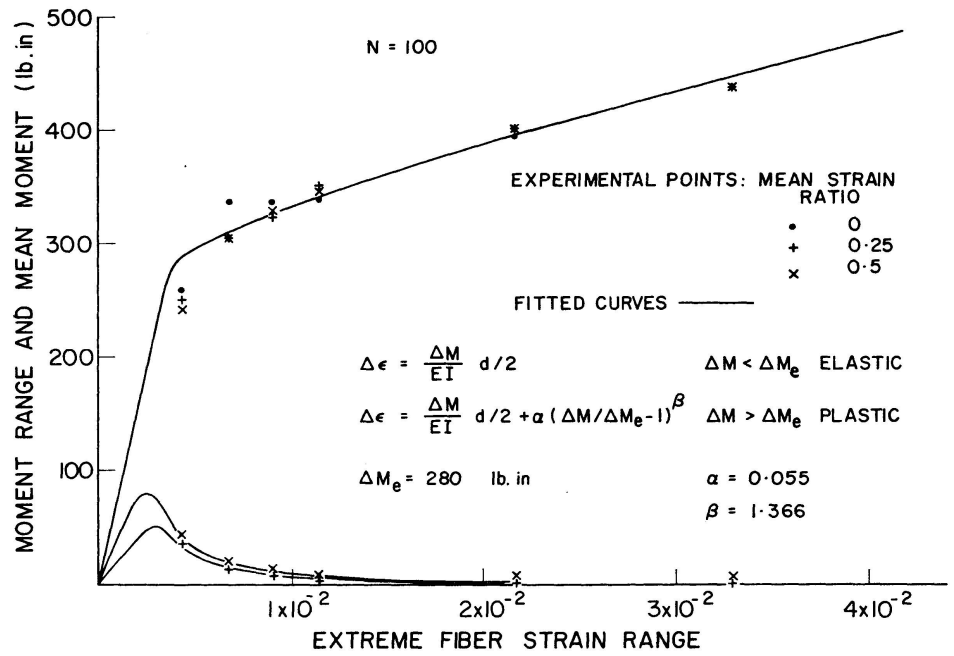

Fig. 10d.

is obtained by cross-plotting the data in Fig. 8 at $N = 100$. The other diagrams of Fig. 10 are derived in a similar way.

A two phase model of the type

$$\Delta\epsilon = \frac{\Delta M}{EI}\frac{d}{2} \qquad \text{for elastic behaviour,} \qquad \text{(I)}$$

$$\Delta\epsilon = \frac{\Delta M}{EI}\frac{d}{2} + \alpha\left(\frac{\Delta M}{\Delta M_e} - 1\right)^{\beta} \qquad \text{for inelastic behaviour} \qquad \text{(II)}$$

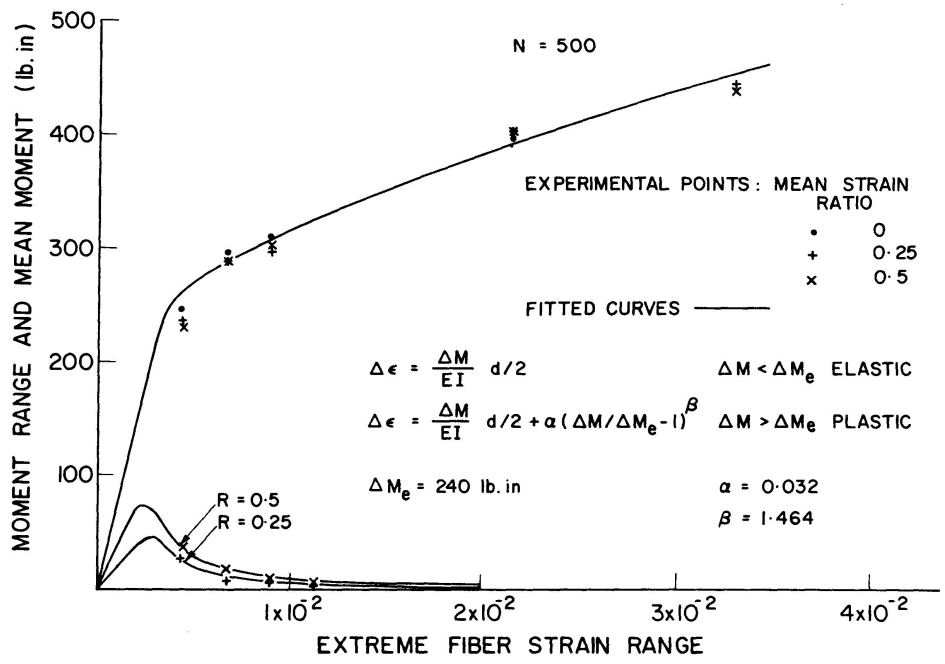

Fig. 10e.

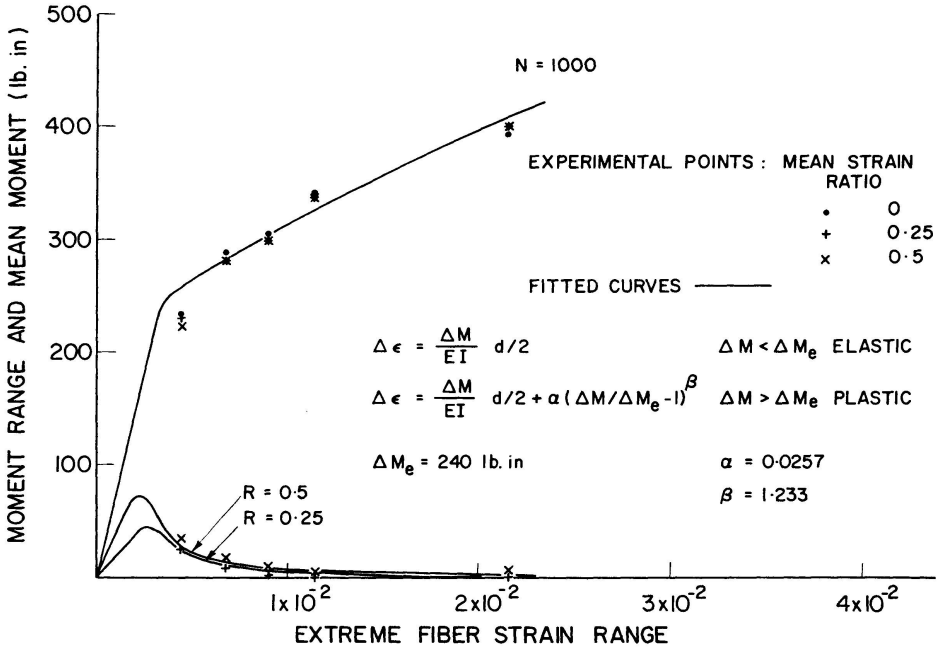

Fig. 10f.

is proposed as a fit to the moment range-strain range data where

$\Delta\epsilon$ = strain range,
ΔM = moment range,
ΔM_e = proportional moment range,
EI = flexural stiffness,
d = depth of section,
α, β = section and material constants.

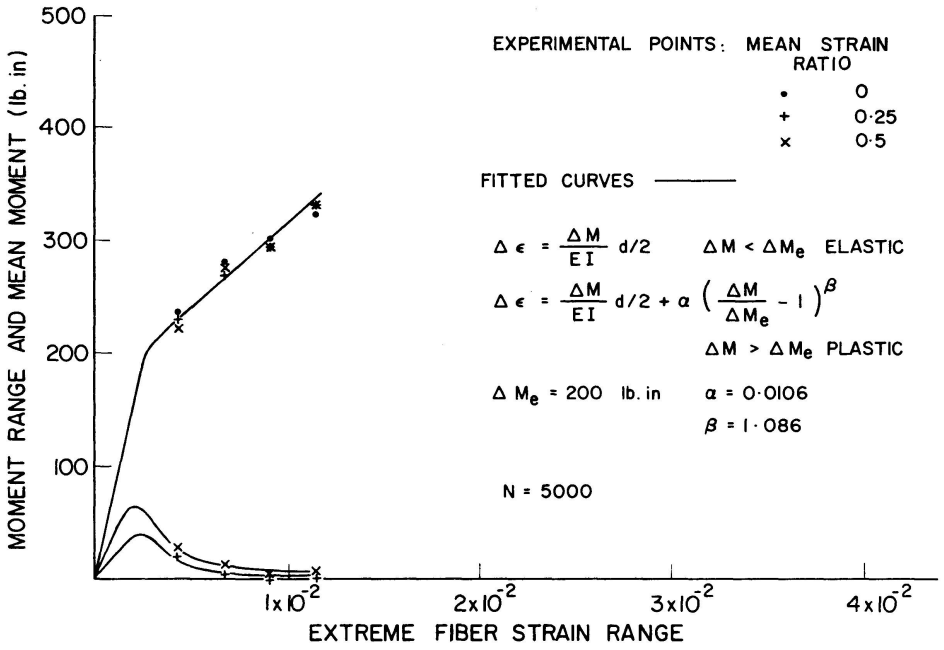

Fig. 10g.

This model is continuous and, as shown in Fig. 10 fits the data reasonably well. Dividing both sides of Eqs. (I) and (II) by $d/2$, leads to a cyclic moment-curvature relationship of the form:

$$\Delta k = \frac{\Delta M}{E I}, \tag{III}$$

$$\Delta k = \frac{\Delta M}{E I} + \frac{2}{d}\alpha\left(\frac{\Delta M}{\Delta M_e} - 1\right)^{\beta}. \tag{IV}$$

Since strain can be considered as dimensionless, the diagrams of Fig. 10 are semi-dimensional (only the moment axis has units) and can be easily employed for any rectangular structural section provided that the applied moment is adjusted by the appropriate ratio of the two section moduli, that of the section in Fig. 10 to that of the particular section under consideration.

The flexural stiffness, EI, for the test section was calculated theoretically from the section geometry and a value of 29.6×10^6 psi for E. The constants α, β and ΔM_e were established from a least squares curve fitting analysis. Thus, for each cyclic stage, a set of values for these constants was established (Appendix II).

The effect of mean strain on the moment range-strain range relation is shown in Fig. 11 for N equal 5 for which the discrepancy is largest. Four fitted curves are shown: three corresponding to the three mean strain ratios and the fourth to an average. The largest discrepancy corresponds to mean strain ratios of 0 and $\frac{1}{2}$ and a strain range of 0.00415. It is less than 15%. The deviation from the average curve, however, is about 8%. For larger strain range

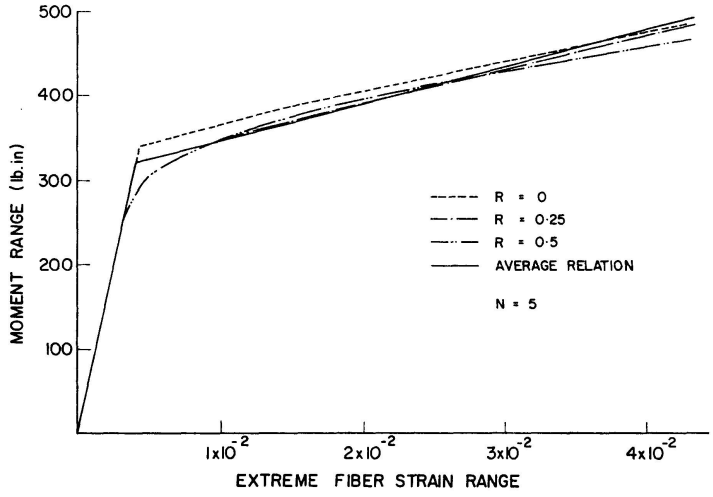

Fig. 11. Effect of Mean Strain on Moment Range-Strain Range Relation.

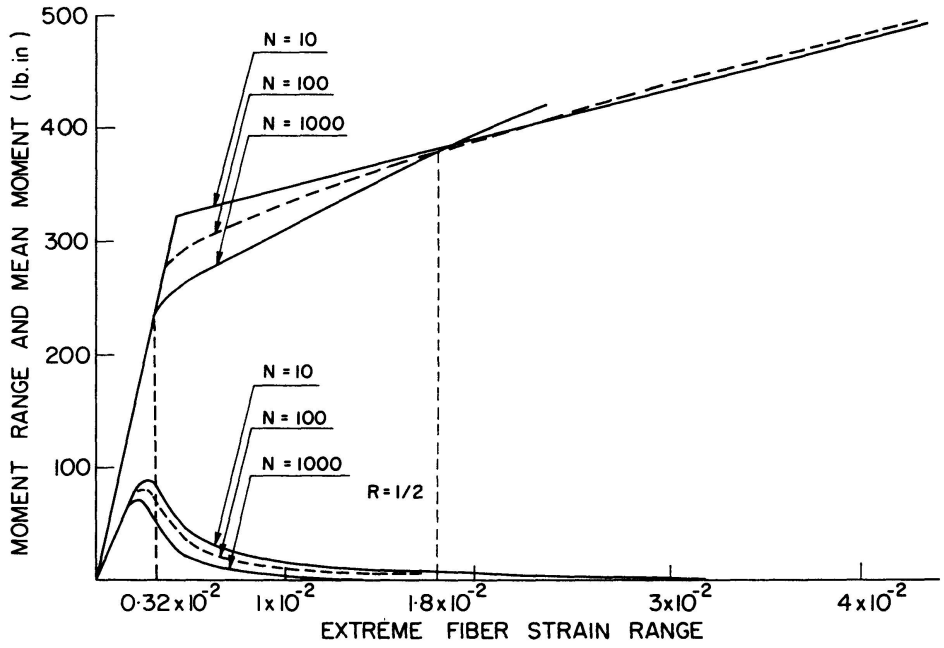

Fig. 12. Aggregated Cyclic Moment-Strain Relations.

value, the variation is not more than 5%. These variations become insignificant when N reaches large values, as discussed previously.

The cyclic softening and hardening characteristics of flexural sections can be visualized by examining the moment range-strain range relation at different cyclic stages. Such relations can be seen in Fig. 12 for $N = 10$ and $N = 1000$. The figure shows three different regions with respect to the extreme fiber strain range: from zero to 0,0032 where the all curves coincide; from 0.0032 to 0.018, where the curve for $N = 1000$ lies below that for $N = 10$, leading to cyclic softening within that range; and the region for strain range greater than about 0.018, where the section hardens with cycling. It is worth noting that, for the particular strain range value of 0.018, the section neither hardens nor softens but remains practically stable (or neutral) throughout its life. The

curves for N between 10 and 1000 cycles lie within the two limiting states of response. One such curve ($N=100$) is shown in dashed lines on the same figure.

Conversely, the mean moment versus strain range relationship poses a more difficult problem. A glance at Fig. 10 reveals that the curve required to fit the data for any mean strain ratio should have three regions: an initial straight line, an intermediate convex curve and finally a concave region where the curve asymptotically approaches zero for large values of curvature range. The slope of the initial straight part is simply equal to that of the initial portion of the $\Delta M - \Delta \epsilon$ relation times the mean strain ratio (ratio of mean strain over strain range). The latter region of the experimental data is modelled by an equation of the form:

$$M_m = \frac{\theta_1}{(\Delta \epsilon)^{\theta_2}}, \tag{V}$$

where M_m is the mean moment and θ_1 and θ_2 are constants to be established by least square analysis. The intermediate range is assumed to have the form:

$$M_m = C_1 + C_2 \Delta \epsilon + C_3 \Delta \epsilon^2 + C_4 \Delta \epsilon^3. \tag{VI}$$

This is a third degree polynomial with four arbitrary constants. From the continuity of the function and its slopes at the first transition point, i.e., between initial and intermediate regions, and the second transition point (between the intermediate and last regions) four equations will be obtained. Solving these equations simultaneously will establish the constants C_1 to C_4. Some approximation was used to locate these two transition points and Appendices III and IV deal with this concept in more detail. Fig. 10 shows the experimental data and the fitted curves.

Behaviour and Models

A total of twenty pure bending tests were conducted. The extreme fiber strain range assumed seven values: the smallest was 0.00428 or 1.36 times the monotonic yield strain range value; the largest was 0.0479 which is very close to the monotonic strain-hardening range value. At each level three tests, comprising a single set, were conducted except for the largest strain range where the set included only two tests. In each set, the first test involved no mean strain; the second included a mean strain equal to one-fourth the strain range; the third test had a mean strain equal to one-half the strain range.

The results of each set of tests were consistent within themselves. The moment range varied little with the introduction of mean strain. Thus, any inconsistency could have been readily identified. A maximum discrepancy of 15% of moment range in one set with a particular strain range is explained in terms of the proportion of plastic strain within the given total strain of the hysteresis loop. The mean moment, on the other hand, increased with the

increase in mean strain for small strain ranges. For large strain range values, however, the increase in mean moment was not that pronounced. In both cases, the experimental findings could be easily explained using the well-known rheological model [12]. The life observed for the tested specimens ranged from 300 cycles to above 100,000 cycles. Thus, most of the low cyclic fatigue range, pertinent to structural design, was covered.

The moment range versus the strain range obtained experimentally has been described by the two phase model of Eqs. (I) and (II). Fig. 10 shows that the suggested model fits the data reasonably well. The model could even be simplified to elastic strain hardening (bi-linear) without much loss of accuracy. However, this simplification was unnecessary since the structural calculations are computerized. The parameter ΔM_e decreased with cycles as did α; in contrast β did not show an amenable trend, hence the moment range-strain range was presented as a discrete function of cyclic life. Also, the mean moment-strain range relation was considered as such. Due to the tri-partite nature of the latter relation there were eight parameters to be established for each mean strain ratio: four in constant C, two in θ and two transition point strain values [Eqs. (V) and (VI)]. If the last two terms of Eq. (VI) were neglected, two parameters would be eliminated. However, the replacement of the third degree curve by a straight line would induce some unwarranted inaccuracy and two discontinuities in the model.

The experimental data revealed that the mean moment decreased rapidly as the strain range increased. Thus for $\Delta \epsilon$ equal to three times the maximum elastic strain range, the mean moment could be neglected, its value being less than 2% of the moment range. Therefore, the value of the mean moment-strain range model is confined to the intermediate domain of strain range, i. e., where the strain range is larger than the limit elastic strain range, for which linear classical theory applies, and smaller than the values associated with negligible mean moment.

Cantilever Beams

Bending Under Unequal Tip Deflection

The behaviour of the cantilever beam shown in Fig. 6 will be predicted theoretically and investigated experimentally in the present study. A single cyclic load is applied at its "tip" to cause cyclic deflections confined to two predetermined values, i. e., the beam is under deflection control. The deflection limits need not be symmetrical; the symmetrical case, however, is studied first in order to develop the method of calculation. The unsymmetrical case will be examined later.

The cantilever is under deflection control. If the associated load is well below the elastic limit of the material, there will be negligible softening or

hardening and section of the beam can be presumed as being under either moment or curvature control. If the load exceeds the linear limit, the sections are under neither moment control nor curvature control but under some mixed control condition. Nonetheless, it seems reasonable to predict cyclic structural behaviour, in this case, from a moment-curvature relationship based on controlled, fixed curvature limits [11]. The basic assumptions made in this investigations are as follows:

1. Inertia forces and weight of specimen are negligible.
2. The effects of shearing stresses can be ignored, arising from the geometry of the specimen as related to load position.
3. Variable cross sections can be idealized as a series of short, discrete segments each having a constant cross-section.
4. Plane sections before bending remain plane after bending.
5. Small deflection theory is applicable.
6. The normalized cyclic moment-curvature relation describes the behaviour of all geometrically similar cross-sections made of the same material.
8. Local and other kinds of buckling are prevented.

Analysis

As presented previously, the cyclic moment range-strain range relation can be regarded as independent of the mean strain. Hence, the cyclic load range-deflection range relationships can be expected to be independent of the mean deflection. The case of symmetrical deflection limits will first be presented and will be followed by consideration of the non-zero mean deflection case.

The method of predicting response is an iterative one; for a given deflection, a load range is assumed and the resulting deflection range is calculated. If this deflection range is equal to that specified, the assumed value of load range is the one sought; if not, the load range is adjusted and the entire process is repeated until convergence is obtained to within the desired error.

To obtain the deflection of the tip of the cantilever under an assumed concentrated load at the same point, the beam is divided into a number of segments. For each segment end and for the depth and width at that segment end, the curvature corresponding to the moment at that location is calculated from the cyclic moment-strain equation and section depth given as input data. Having established the curvatures at successive locations along the length of the beam, the "elastic curve" can be constructed. Elementary mathematics yield the deflection at any segment end of the beam. Appendix V presents the mathematical operations involved. Table I describes the main steps of a computer program based on the method presented herein.

For the cantilever beam under unequal deflection limits the method is a little more involved. The input data should include the mean deflection range.

Table I. Flow Chart

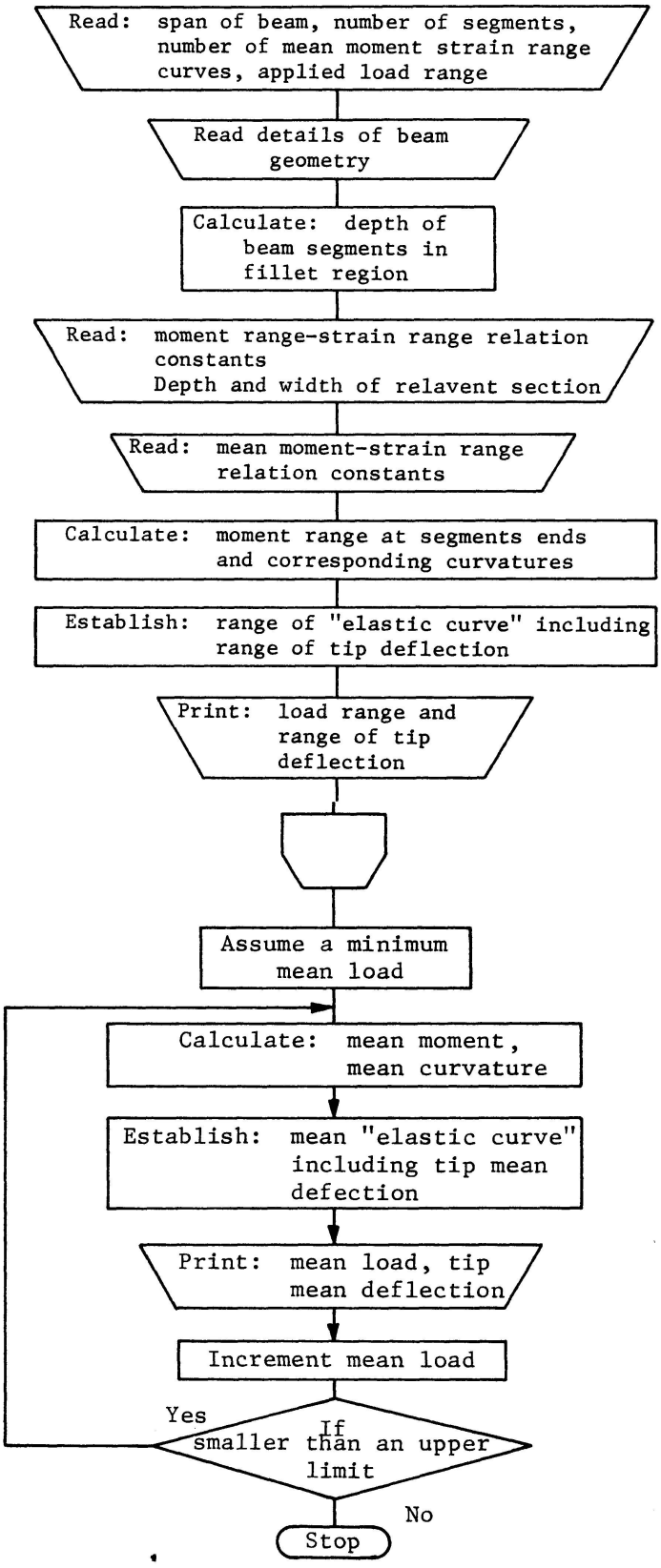

The desired values, on the other hand, are the corresponding load range and mean load. A trial mean load is first assumed and the corresponding mean deflection is calculated. If this mean deflection is equal to the specified mean deflection to within the tolerable error, the assumed value of load is accepted; otherwise, the assumed mean load is adjusted until the corresponding mean deflection converges to the specified value. The method presented for the calculation of deflection range is used again to calculate the mean deflection with one difference; the curvature range (or extreme fiber strain range) at the end of each beam segment is replaced by the mean curvature or mean strain at the same location.

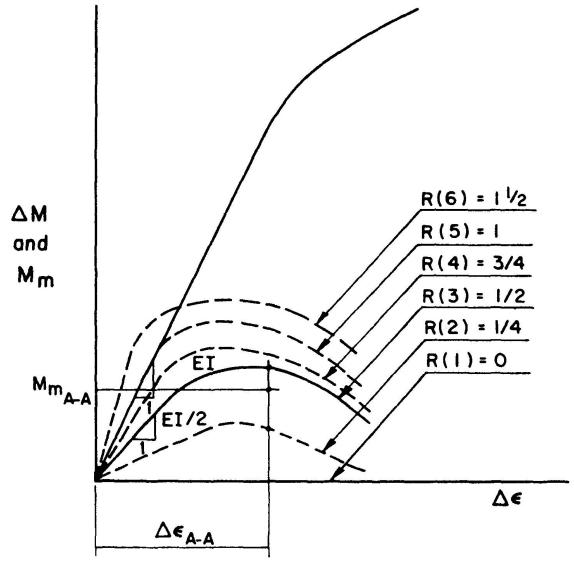

Fig. 13. Schematic Interpolation for Mean Strain.

For the calculation of this mean strain at a certain section, designated $A-A$, it is necessary to have at hand the strain range established from load range calculations and the mean moment calculated from the assumed mean load at the same section. These values are designated by $\Delta\epsilon_{A-A}$ and $M_{m_{A-A}}$ respectively. Fig. 13 shows the moment range and mean moment-strain range relations with the X axis distorted for the sake of clarity. Now, the mean moment value corresponding to a strain range of $\Delta\epsilon_{A-A}$ and a mean strain ratio equal to $R(I)$ is established, I being 2 for the first attempt. If the resulting mean moment is larger than $M_{m_{A-A}}$, the actual mean strain ratio is interpolated linearly between $R(I)$ and $R(I-1)$; if smaller, I is increased until the desired condition is met. Thus, the product of the interpolated mean strain ratio and strain range is an approximation to the desired mean strain. The mean curvature is simply the mean strain over half the beam depth.

Results and Discussion

Nine tests were conducted on cantilever beam, four pairs and a single. Each pair of beams had a single deflection range; one beam had no mean deflection

and the other had a mean deflection equal to about one eighth of the deflection range, i. e., completely and partially reversed deflections.

The deflection range for the first pair was 0.17″. The strain range at the critical section at the fifth cycle was, as obtained from the computer program, equal to 0.0034. This was less than the limiting linear strain range at the same cyclic state which was equal to 0.00415, Fig. 10a. Therefore, and since the material did not harden from the first to the fifth cycle for that strain range, the completely reversed deflection beam remained elastic up to at least the fifth cycle. Assuming the same conclusion was applicable to the partially reversed deflection case, the mean strain ratio would be equal to the mean deflection ratio, i. e., about one eighth. The maximum strain amplitude calculated on this basis, however, was found to be slightly higher than the maximum linear strain amplitude. Hence, the second beam has undergone some plastic deformation. This was readily observed from the hysteresis loop which was a straight line for the first beam and had some width for the second beam at the cyclic state under consideration.

As cycling progressed, the material softened. At $N = 5000$, for example, the limit linear strain range dropped to 0.00261 whereas the strain range at the critical section increased to about 0.0044. Naturally, both beams had undergone some plastic deformation although this was limited to small lengths along the beam. This conclusion was again supported by observations on the relevant hysteresis loops. The failure of the beam under zero mean deflection took place after 105,000 cycles; the test on the second beam was halted at

Fig. 14a–e. Experimental Versus Theoretical Results.

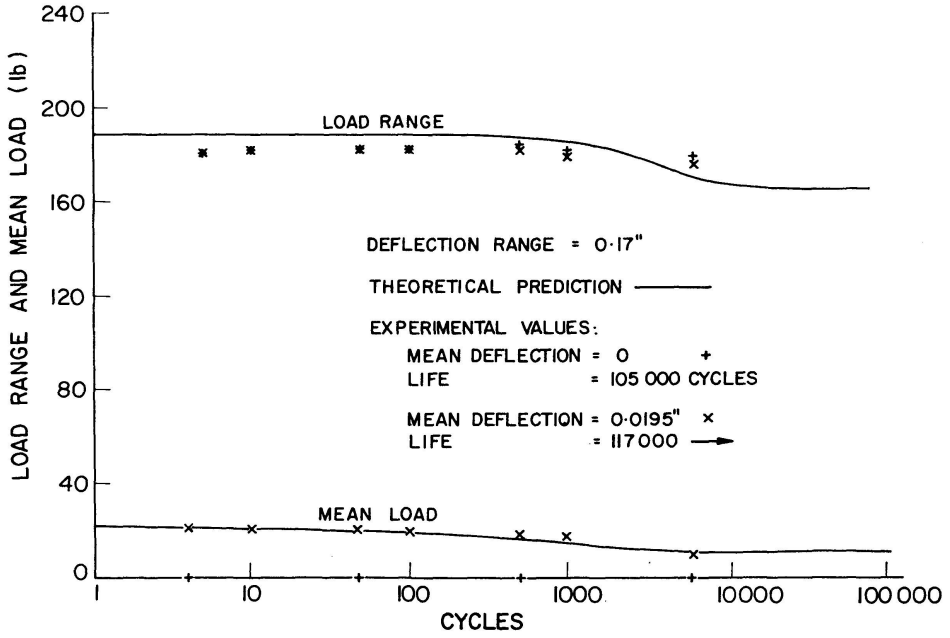

Fig. 14a.

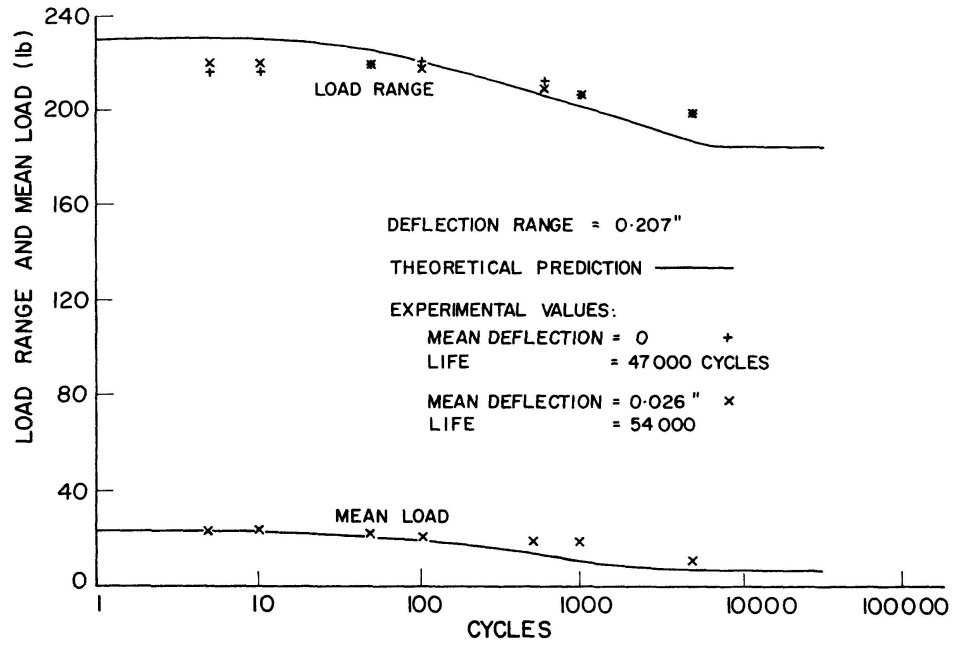

Fig. 14b.

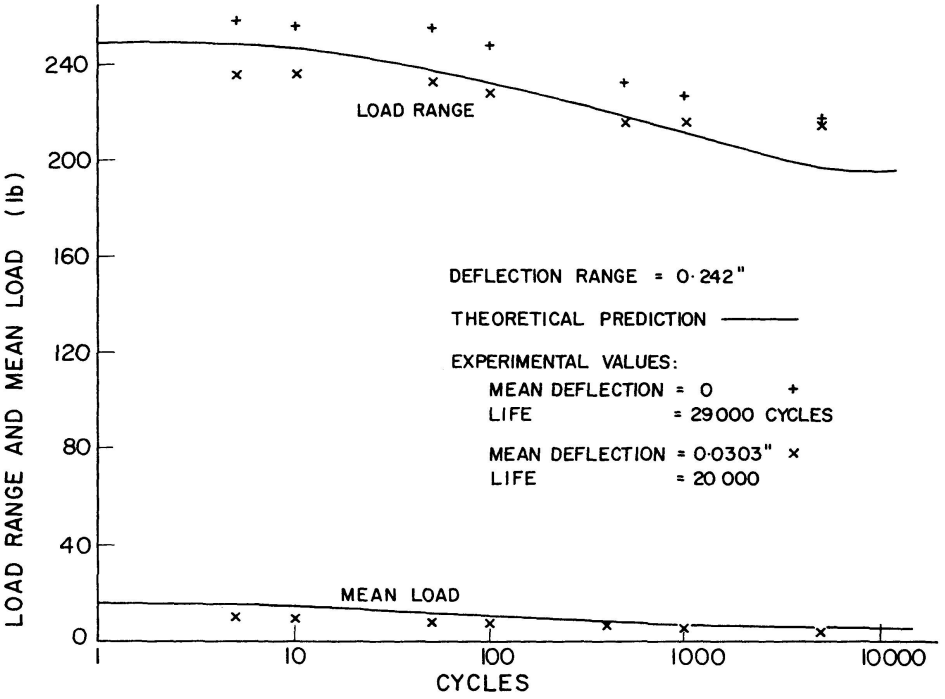

Fig. 14c.

117,000 cycles and failure was not attained. Hence, this deflection range may be considered to promote conventional fatigue.

For this deflection range Fig. 14a shows the theoretical load range and mean load versus cyclic life. The two solid lines were obtained by connecting discrete theoretical points corresponding to cycles 5, 10, 50, 100, 500, 1000 and 5000. The experimental results are also shown as discrete point at the above-mentioned cyclic states.

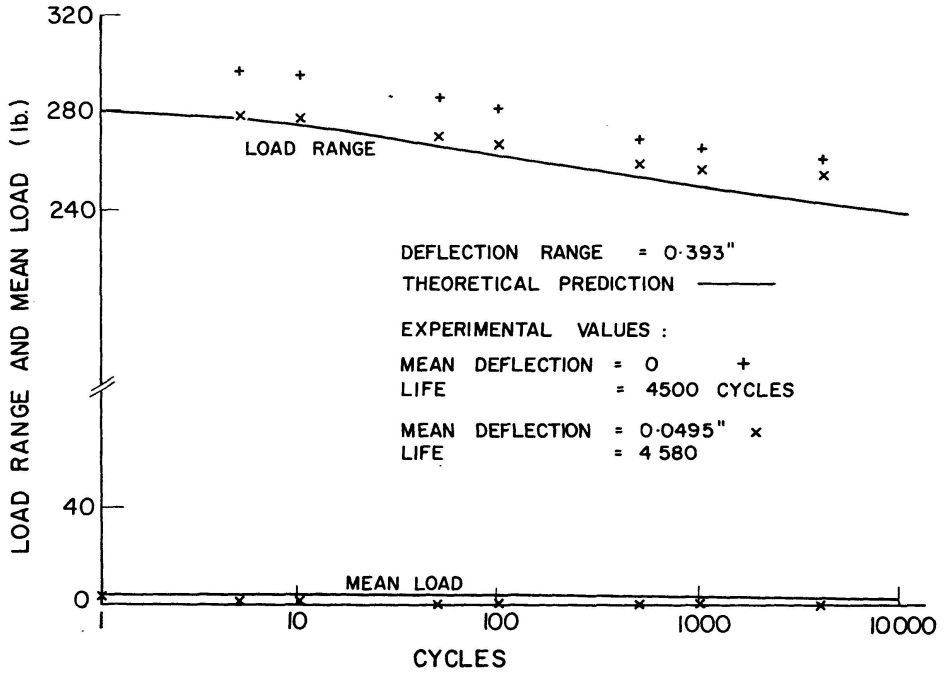

Fig. 14d.

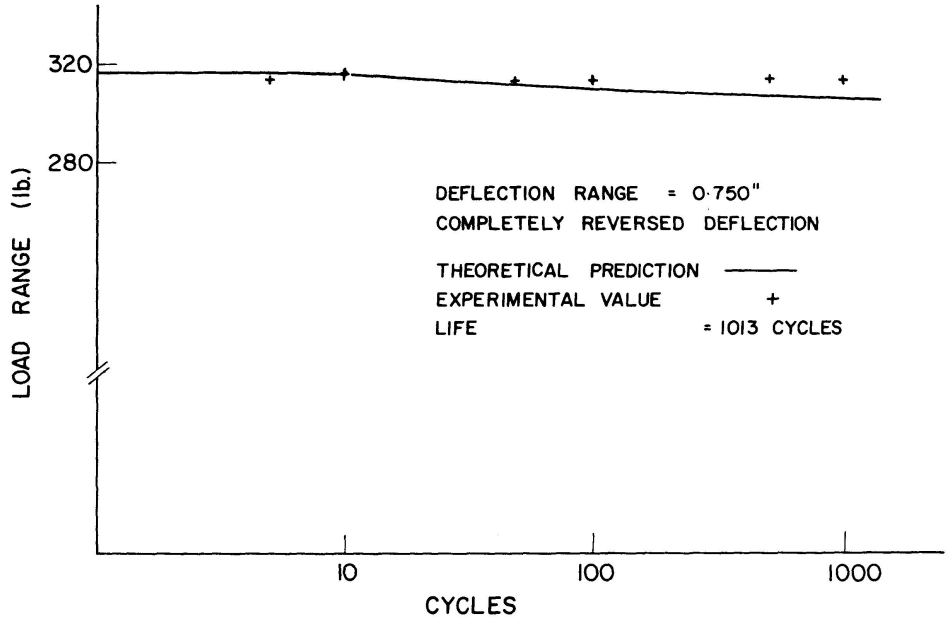

Fig. 14e.

In a similar manner, Figs. 14b, 14c, 14d and 14e show the theoretical and experimental results as well as life span for four larger deflection ranges equal to 0.207″, 0.242″, 0.393″ and 0.750″. It can be seen that the experimental load range associated with the smallest deflection range, Fig. 14a was not significantly influenced by mean deflection – the maximum relative discrepancy was about 3% at $N=5000$. Among all the deflection ranges, the maximum discrepancy occurred in the case of deflection range equal to 0.242″ and $N=5$. This discrepancy was 9% or a variation of less than 5% from the average

value. For the deflection ranges equal to 0.207″ and 0.242″, the variation was not more than 4% measures about the average. It is worth noting here that the experimental load range for zero mean deflection was, in general, larger than that for non-zero mean deflection. The discrepancy of 9% is less than the value of 15% presented previously in the discussion of the effect of mean strain on the moment-strain relation. This is due to the fact that the structural behaviour is an aggregate of sectional behaviour and that only at the critical section the mean strain ratio approaches the value of $\frac{1}{2}$ for the large deflection ranges.

For the largest deflection range of 0.75″, the maximum strain at the critical section was 0.034 at the fifth cycle and dropped to 0.023 at $N = 1000$. Both strain values are lower than the maximum value investigated under pure bending. Larger deflections, that will cause larger strain ranges, were not investigated as the effects of geometry change leading to membrane action cease to be insignificant for such deflections; the consideration of the effects of geometry change falls outside the domain of the current work.

The difference between the theoretical load range and the averaged experimental one, on the other hand, compared fairly well, the maximum difference being not more than 4% for any deflection range. It can be seen that the theoretical predictions are closer, in general, to the experimental results for non-zero mean deflection case than to the zero mean deflection one. This can be explained with reference to Fig. 11 which shows that the average moment range-strain range fits the partially reversed or repeated strain cases better than the completely reversed case. But since the error involved is fairly small, neglecting the effect of mean strain on moment range under pure moment and on load range under deflection control can be easily justified.

The theoretical and experimental mean load values, on the other hand, compare fairly well as shown in Fig. 14, especially when they are most significant, i.e., over the three lowest deflection ranges. When the mean load is added to and subtracted from half the load range, the maximum and minimum load limits are obtained, respectively. Simple calculations show that the relative error between theoretical prediction and experimental value for these limits is less than 5%.

Conclusions

Cyclic moment-strain relations, based upon deformation control tests conducted on rectangular structural steel sections were established. A model describing the moment range versus extreme fibre strain range, independent of the mean strain value, is presented. A second suggested model describes the mean moment versus the extreme fiber strain range for different ratios of mean strain over strain range at the same fiber. These models reduce cyclic flexural behaviour of sections to a pseudo-static representation amenable for

use in cyclic structural analysis. These models are capable of accommodating, in discrete form, the phenomena of hardening and softening of aggregations of fibres constituting a structural section as well as relaxation of mean moment.

A number of tests were conducted on cantilever beam specimens under tip deflection control. The behaviour under completely and partially reversed deflections was investigated. The load range was found to be little influenced by the mean deflection. Also, the mean load relaxed to an insignificant value in the first cycle when the deflection range was large enough to cause appreciable cyclic plastic deformation. For such cases, then, the beam could be considered as cycled under completely reversed deflection with a rest condition corresponding to the mean deflection position.

A theory was developed and presented for the prediction of the behaviour of such beams. It employs a discrete curvature-area method coupled with the cyclic moment-strain relations described above. The theoretical results agree fairly closely with experimental values. The theory also confirmed that the behaviour of simple structures under cyclic deformation can be divided into three cases, comprising: (1) an elastic case where the mean load is proportional to the load range; (2) an intermediate range where proportionality does not apply and the effect of mean deflection (mean load) cannot be ignored, and (3) the case of large, inelastic cyclic deformation where the effects of mean deflection can be completely ignored except for associated changes in structural geometry and its secondary membrane effects.

Notation

$\Delta \epsilon$	strain range.
ΔM	moment range.
ΔM_e	proportional moment range.
EI	flexural stiffness.
d	depth of section.
α, β	section and material constants.
Δk	curvature range.
M_m	mean moment.
$\theta_1, \theta_2,$ $C_1, \ldots C_4$	constants of mean moment-strain range relation.
R	ratio of mean strain over strain range or, ratio of mean curvature over curvature range.

Acknowledgements

This investigation was carried out in the Department of Civil Engineering at the University of Waterloo with financial assistance from the National Research Council of Canada under grant A-1582.

Appendix I. Depth of Cantilever Beam

Consider the cantilever beam specimen shown in Fig. I.1. Assuming that the upper fillet has a constant radius of curvature equal to R_1 it is required to determine the distance y in terms of x_1, x_2, R_1 and R_2.

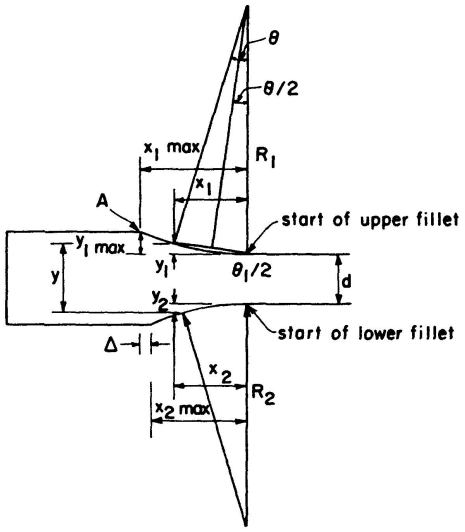

Fig. I.1. Cantilever Beam Fillet Depth.

From the Fig. I.1, obtain

$$x_1 = R_1 \sin\theta$$

or
$$\theta = \sin^{-1}\frac{x_1}{R_1},$$

also
$$y_1 = x_1 \tan\left(\frac{\theta}{2}\right),$$

then
$$y_1 = x_1 \tan\left(0.5 \sin^{-1}\frac{x_1}{R_1}\right). \tag{I.1}$$

Similarly,
$$y_2 = x_2 \tan\left(0.5 \sin^{-1}\frac{x_2}{R_2}\right)$$

and
$$y = y_1 + y_2 + d. \tag{I.2}$$

Hence, the depth of the section can be given as a function of the section location and the fillet radii.

The point where the fillet begins is usually difficult to establish by measurement accurately. Eq. (I.1) is used for this purpose as follows: for point A, y_{1max} can be easily measured. Assume a value for x_{1max} and calculate the corresponding y_1; if equal to the measured value of y_{1max}, the answer is obtained; if not, change the assumed value of x_{1max} until convergence is obtained. x_{2max} can be established similarly. A very short computer program facilitates such calculations.

For all specimen tested, R_1 and R_2 on the one hand and x_{1max} and x_{2max} on the other were close to each other. Also Δ was very small. In consequence, the assumption that the neutral axis of the untested specimen is a straight line is quite acceptable.

Appendix II. Determination of Coefficients (α, β, ΔM_e)

Assume a relationship of the form:

$$\Delta\epsilon = \frac{\Delta M}{EI}\frac{d}{2} \qquad \text{for the linear range where } \Delta M \leqq \Delta M_e \tag{II.1}$$

and

$$\Delta\epsilon = \frac{\Delta M}{EI}\frac{d}{2} + \alpha\left(\frac{\Delta M}{\Delta M_e} - 1\right)^{\beta} \qquad \text{for the non-linear range where } M > \Delta M_e. \tag{II.2}$$

The experiments provide a set of values $\Delta\epsilon$ and ΔM for each cycle, N. The coefficients will be evaluated so as to minimize the sum of the squares of the deviations of test points from an average curve. The curve fitting will be applied to the non-linear range only since the initial slope is considered fixed; but the limit of the linear range will be considered as a variable. The data point or points within the linear range will not be considered in the following step.

Eq. (II.2) can be rewritten in the logarithmic form as

$$\mathrm{Log}\left(\Delta\epsilon - \frac{\Delta M}{EI}\frac{d}{2}\right) = \mathrm{Log}\,\alpha + \beta\,\mathrm{Log}\left(\frac{\Delta M}{\Delta M_e} - 1\right)$$

or

$$y = K_1 + K_2 x, \tag{II.3}$$

where

$$y = \mathrm{Log}\left(\Delta\epsilon - \frac{\Delta M}{EI}\frac{d}{2}\right),$$

$$x = \mathrm{Log}\left(\frac{\Delta M}{\Delta M_e} - 1\right),$$

$$K_1 = \mathrm{Log}\,\alpha,$$

$$K_2 = \beta.$$

First ΔM_e is assumed constant. Thus, the problem is reduced to establishing two coefficients rather than three.

The least square analysis implies minimization of

$$E = \sum_{i=1}^{n} (y_i - K_2 x_i - K_1)^2.$$

Differentiating with respect to K_2 and K_1 for minima

$$\frac{\partial E}{\partial K_2} \rightarrow \sum_{i=1}^{n} (x_i y_i - K_2 x_i^2 - K_1 x_i) = 0,$$

$$\frac{\partial E}{\partial K_1} \rightarrow \sum_{i=1}^{n} (y_i - K_2 x_i - K_1) = 0$$

or
$$K_1 \sum_{i=1}^{n} x_i + K_2 \sum_{i=1}^{n} x_i^2 - \sum_{i=1}^{n} x_i y_i = 0, \tag{II.4}$$

$$K_1 \cdot 1 + K_2 \sum_{i=1}^{n} x_i - \sum_{i=1}^{n} y_i = 0, \tag{II.5}$$

where
$$K_1 \sum_{i=1}^{n} 1 = K_1 n.$$

The values of K_1 and K_2 are obtained by solving Eqs. (II.4) and (II.5).

$$K_2 = \frac{n \sum_{i=1}^{n} x_i y_i - \sum_{i=1}^{n} y_i \sum_{i=1}^{n} x_i}{n \sum_{i=1}^{n} x_i^2 - \sum_{i=1}^{n} x_i \sum_{i=1}^{n} x_i}$$

and
$$K_2 = \frac{\sum_{i=1}^{n} x_i^2 \sum_{i=1}^{n} y_i - \sum_{i=1}^{n} x_i \sum_{i=1}^{n} x_i y_i}{n \sum_{i=1}^{n} x_i^2 - \sum_{i=1}^{n} x_i \sum_{i=1}^{n} x_i}.$$

Having established K_1 and K_2, and, therefore α and β, the sum of the square of deviations can be given as

$$S = \sum_{i=1}^{n} \left[\Delta \epsilon - \frac{\Delta M_i}{E I} \frac{d}{2} - \left(\frac{\Delta M_i}{\Delta M_e} - 1 \right)^{\beta} \right]^2. \tag{II.5}$$

In this summation, all experimental data points should be included, be they below the elastic limit or above it, with due attention being paid to including or excluding the third term in Eq. (II.5).

Repeating the whole process but for a different value of ΔM_e, a new value for S is obtained, The best value of ΔM_e and the associated α and β are those which give the smallest value of S. The process, therefore, is complete when the minimum of $S = f(\Delta M_e)$ is obtained. This was programmed quite simply on a computer.

Appendix III. Location of First Transition Point

Assume the monotonic moment-curvature relation as given in Fig. III.1 where $\frac{\Delta M_e}{2}$ is the limit linear moment and k_0 is the corresponding curvature. When cycling with zero mean curvature, the loop will generally have a plastic component (and width) only if the curvature range exceeds $2k_0$. On the other hand, for a loop with constant mean curvature ratio, the mean moment will increase linearly with increase in curvature range as long as the absolute maximum curvature is less than k_0. Fig. III.2 illustrates such a case for mean curvature ratio of 1/2. Whenever the maximum curvature exceeds k_0, the mean moment ceases to increase linearly with curvature range. Therefore,

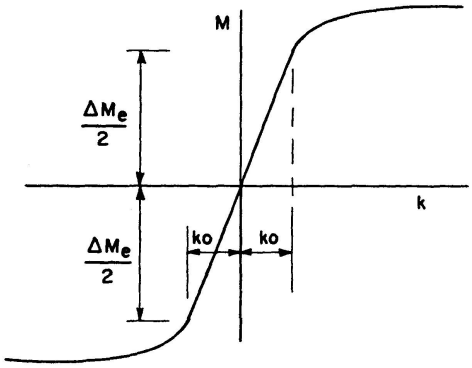

Fig. III.1. Maximum Linear Curvature.

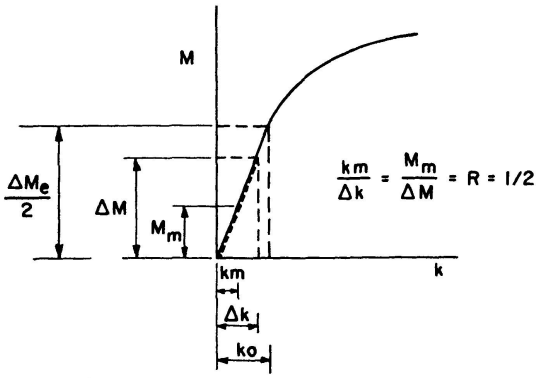

Fig. III.2. Calculation of Elastic Mean Moment Value.

the limit state is given by

$$k_{max} \leqq k_0 .$$

But

$$k_{max} = \frac{\Delta k}{2} + k_m ,$$

where Δk is curvature range and k_m is mean curvature

$$k_{max} = \frac{\Delta k}{2} + R \Delta k ,$$

where R is a ratio of proportionality

or

$$k_{max} = \Delta k \left(\tfrac{1}{2} + R\right),$$

$$\Delta k = \frac{k_{max}}{\tfrac{1}{2} + R},$$

when k_{max} assume its limit linear value, k_0, we obtain

$$\Delta k_{max} = \frac{k_0}{\tfrac{1}{2} + R}. \tag{III.1}$$

In other words, the maximum curvature range, for which the mean moment remains proportional to the mean curvature, is inversely proportional to $(\frac{1}{2} + R)$. The mean moment at this limit is designated the Maximum Linear Mean Moment (MLMM). Since it is at the limit of the linear range, it is given by:

$$\text{MLMM} = (\text{slope}) \cdot (\text{limit curvature}).$$

Since the slope is equal to $(E\,I\,R)$

$$MLMM = (E\,I\,R)\frac{k_0}{\tfrac{1}{2} + R} = \frac{\Delta M_e}{2}\frac{R}{\tfrac{1}{2} + R} \cdots \tag{III.2}$$

By solving Eq. (III.1) for R and substituting in Eq. (II.2), we obtain

$$R = \frac{k_0}{\Delta k_{max}} - \frac{1}{2}$$

and
$$MLMM = \frac{M_e}{2} \frac{\frac{k_0}{\Delta k_{max}} - \frac{1}{2}}{\frac{1}{2} + \frac{k_0}{\Delta k_{max}} - \frac{1}{2}} = \frac{\Delta M_e}{2}\left(1 - \frac{\Delta k_{max}}{2 k_0}\right) \qquad \text{(III.3)}$$

or
$$MLMM = A(1 - Bx),$$

where
$$A = \frac{\Delta M_e}{2}, \qquad B = \frac{1}{2 k_0}, \qquad x = \Delta k_{max}.$$

Eq. (III.3) describes a straight line passing through the points $\left(0, \frac{\Delta M_0}{2}\right)$ and $(2 k_0, 0)$ as shown in Fig. III.3.

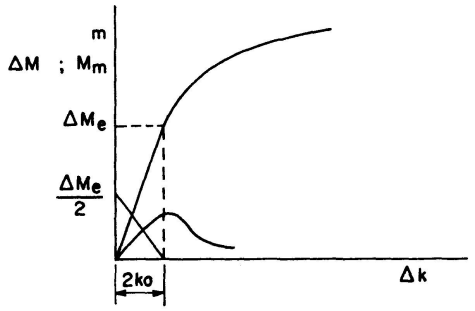

Fig. III.3. Limiting Linear Curvature.

The above discussion is applicable only to the case where ΔM_e is constant. However, as the specimen is cycled, the maximum linear moment range decreases due to the initiation of localized plastic strain. This will, in turn, cause the mean moment to decrease with cycling; therefore, the maximum linear mean moment will also decrease with cycling.

It does not seem unreasonable, then, to assume that the maximum linear mean moment locus will continue to be a straight line intersecting the curvature range axis at $2 k_{0n}$ and the moment axis at $\Delta M_{en}/2$ where k_{0n} and ΔM_{en} are similar to k_0 and ΔM_e but corresponding to cycle N. Therefore, this straight line locus will move parallel to itself with cycling.

Finally, what has been presented above can also be applied to the moment-strain relation with appropriate substitution of the curvature axis by the strain axis.

Appendix IV. Curve Fitting

The experimental data of the mean moment-extreme fiber relation will be fitted by a curve composed of three regions:

1. A straight line passing through the point of origin and having a slope equal to the product of the initial slope of the $M - \Delta\epsilon$ diagram and the mean strain ratio. The upper limit of this region is a point which has, as locus, a straight line as shown in Fig. IV.1 and explained in Appendix III.

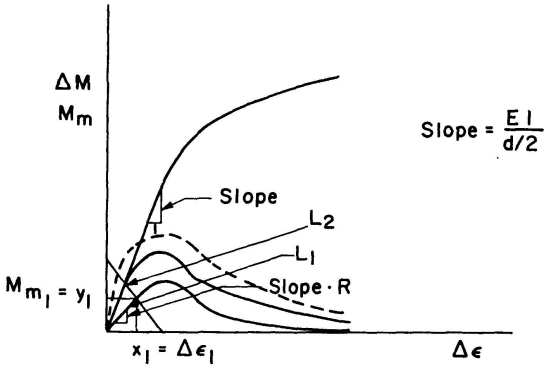

Fig. IV.1. Limiting Linear Mean Moment.

2. A third region where the value of the mean moment approaches zero asymptotically as the extreme fiber strain range reaches high values.
3. An intermediate region bridging the gap between the first and the last regions.

The first region has the form:

$$M_m = \Delta\epsilon \text{ slope } R,$$

where the slope is that of the initial $\Delta M - \Delta\epsilon$ curve $= \frac{EI}{d/2}$, and R is the mean strain ratio. Alternatively,

$$y = x \text{ slope } R, \tag{IV.1}$$

where

$$y = M_m,$$
$$x = \Delta\epsilon.$$

Hence

$$y' = \text{slope } R. \tag{IV.2}$$

The third region is fitted by a curve of the form:

$$M_m = \frac{\theta_1}{(\Delta\epsilon)^{\theta_2}}$$

or

$$y = \theta_1 x^{-\theta_2}, \tag{IV.3}$$

which is a hyperbola with two orthogonal asymptotes, the x and y axes. The two parameters, θ_1 and θ_2 are established using a library subroutine which performs a least squares curve fitting analysis on the input data. The data should include only those points that belong to the region under consideration. The input point with the minimum strain range value is considered common to both second and third regions. Since the fitted curve will not ordinarily pass through the data points, the transition point is considered a point on the fitted curve corresponding to the minimum input strain range value.

Having established the curve parameters and the transition point between the intermediate and third regions, the slope at this point can be calculated by differentiating Eq. (IV.3) with respect to x, i.e.,

$$y' = -\theta_2 \theta_1 x^{-\theta_2 - 1}. \tag{IV.4}$$

Similarly, there is another transition point between the first and intermediate regions. For the continuity of the entire curve, the intermediate range function is to satisfy four conditions, two from the function value at the two transition points and two from the slope at the same points. The third degree function given below has four parameters and can satisfy all four conditions:

$$y = a_0 + a_1 x + a_2 x^2 + a_3 x^3 \tag{IV.5}$$

and

$$y' = a_1 + 2a_2 x + 3a_3 x^2. \tag{IV.6}$$

A lower order function will not provide the desired continuity. Conversely, a higher order function will not be justified unless there are enough additional conditions (experimental data points in the intermediate region) and provided that the resulting curve is smooth and has single curvature.

To establish the first transition point, the intersection of lines L_1 and L_2 in Fig. IV.1 should be located as follows.

For L_1

$$y = x \,\text{slope}\, R. \tag{IV.1}$$

For L_2

$$y = \frac{\Delta M_e}{2} - \frac{x \,\text{slope}}{2}. \tag{IV.7}$$

The point of intersection will be given by

$$x \,\text{slope}\, R = \frac{\Delta M_e}{2} - \frac{x \,\text{slope}}{2}$$

or

$$x_1 = \frac{\Delta M_e}{\text{slope}} \quad \frac{1}{2\,(R+\frac{1}{2})}$$

and

$$y_1 = \frac{\Delta M_e}{\text{slope}} \frac{1}{2\,(R+\frac{1}{2})} \text{slope}\, R = \Delta M_e \frac{R}{2\,(R+\frac{1}{2})}. \tag{IV.8}$$

At x_1 and using Eqs. (IV.8) and (IV.5) obtain

$$a_0 + a_1 x_1 + a_2 x_1^2 + a_3 x_1^3 = \Delta M_e \frac{R}{2\,(R+\frac{1}{2})} \tag{IV.9}$$

and from Eqs. (IV.2) and (IV.6) obtain

$$a_1 + 2a_2 x_1 + 3a_3 x_1^2 = \text{slope}\, R. \tag{IV.10}$$

Similarly, at x_2, using Eqs. (IV.3) and (IV.5) obtain

$$a_0 + a_1 x_1 + a_2 x_1^2 + a_3 x_1^3 = \theta_1 x_1^{-\theta_2} \tag{IV.11}$$

and from Eqs. (IV.4) and (IV.6) obtain

$$a_1 + 2a_2 x_1 + 3a_3 x_1 = -\theta_1 \theta_3 x_2^{-\theta_2 - 1}. \tag{IV.12}$$

Hence, the four unknowns, a_0, a_1, a_2, a_3 can be established by solving Eqs. (IV.9), (IV.10), (IV.11), and (IV.12) simultaneously.

Appendix V. Deflection Calculations

Moment Range

For a load range applied at the tip of the cantilever, the moment range value at any section is equal to the load range times the (perpendicular) distance of the section from the load.

Curvature

The input moment range-extreme fibre strain range relation as shown in Eqs. (I) and (II) is for a rectangular section ($b_0 d_0$) whereas the beam, in general, has a section ($b_x d_x$) at any given location. The units of the left side of the Eqs. are moment units and those for the right side are strain units, i. e., in/in or dimensionless.

A moment range ΔM_x acting on a section ($b_x d_x$) is equivalent to a moment range $\Delta M_x (b_0 d_0^2)/(b_x d_x^2)$ acting on a section ($b_0 d_0$). The extreme fibre strain will be the same for both sections under the appropriate moments. The curvature range, Δk, is simply $(\Delta \epsilon_x)/(d_x/2)$.

Deflections

The curvature-area method will be used. The beam is divided into a suitable number of short segments for which the curvature diagram is assumed linear for each segment, Fig. V.1a, and is divided into two triangles as shown in Fig. V.1b. At the built end, the deflection and slope are zero. The deflection at the right end of each segment has, in general, three components as shown in Fig. V.2: the first is the deflection at the left end, the second is equal to the slope at that end times the segment length and the third is the tangential deviation of the right end with respect to a tangent at the left end. Thus,

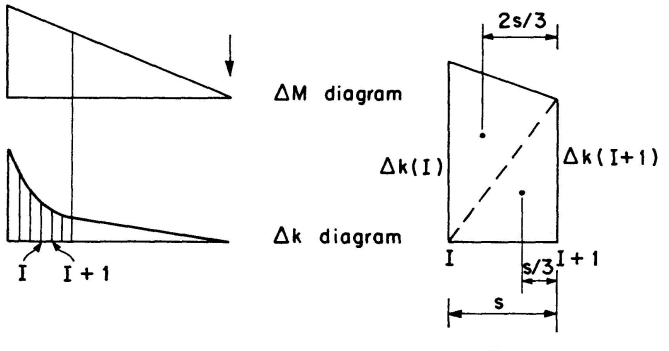

Fig. V.1. Curvature Distribution Diagram.

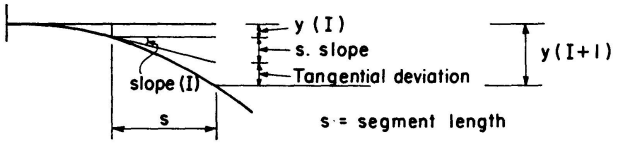

Fig. V.2. Slope and Deflection Calculations.

with the help of Figs. V.1b and V.2, the segment right end deflection and slope can be written as:

$$y(I+1) = y(I) + s\,\text{slope}(I) + \frac{\Delta k(I)\,s}{2}\frac{2}{3}s + \frac{\Delta k(I+1)\,s}{2}\frac{1}{3}s,$$

$$\text{slope}(I+1) = \text{slope}(I) + \frac{\Delta k(I)+\Delta k(I+1)}{2}s.$$

Starting at the extreme left end and moving to the right, discrete points on the "elastic curve" are established up to and including the cantilever tip.

References

1. Neal, B. G.: The Plastic Methods of Structural Analysis. Champan and Hall.
2. Neal, B. G., and Symunds, P. S.: Cyclic Loading of Portal Frames, Theory and Tests. Vol. 18, Pub. IABSE, Zurich, 1958.
3. Popov, E. P., and McCarthy, R. E.: Deflection Stability of Frames Under Repeated Loading. Journal of E. M. Division, ASCE, January, 1960.
4. Royles, R.: Fatigue of Ductile Structures in Reversed Bending. Ph. D. Thesis, Cambridge University, 1964.
5. Sherbourne, A. N., and Krishnasamy, S.: Moment-Curvature Models Under Reversed Cyclic Straining. Experimental Mechanics, Vol. 9, No. 1, 1969.
6. Topper, T. H.: Cyclic Plastic Loading of Mild Steel. Ph. D. Thesis, Cambridge University, 1962.
7. Krishnasamy, S., Sherbourne, A. N., and Khurana, K. K.: Deflection of Mild Steel Beams Under Symmetric Alternating Load. Presented at 1972 SESA Spring Meeting, Cleveland, Ohio, May 23–26.
8. Keshavan, S.: Some Studies on the Deformation and Fracture of Normalised Mild Steel under Cyclic Conditions. Ph. D. Thesis, University of Waterloo, 1967.
9. Jhansale, H. R., and Topper, T. H.: Equipment for Cyclic Deformation and Fatigue Studies in Pure Bending. Presented at 1970 SESA Fall Meeting, Boston, Mass., October 18–22.
10. Topper, T. H. et al.: Fatigue Testing Techniques for Conditions of Biaxial Stress, Stress Concentration, and Pure Bending. Journal of Materials, Vol. 6, No. 4, 1971.
11. Krishnasamy, S.: Beams Under Cyclis Alternating Deflection. Ph. D. Thesis, University of Waterloo, 1966.
12. Martin, J. F., Topper, T. H., and Sinclair, G. M.: Computer Based Simulation of Cyclic Stress-Strain Behaviour with Application to Fatigue. Materials Research and Standards, MTRSA, Vol. 11, No. 2, P. 23.

Summary

The response of simple mild steel cantilever beams to cyclic unequal deflections is investigated theoretically and experimentally following the derivation of appropriate moment-curvature models from strain control data involving the testing of specimens in pure bending. Different models are proposed

relating the curvature to moment range and mean moment; the models can accommodate hardening and softening of aggregations of fibres in the structural cross-section as well as mean moment relaxation with time. It is shown that behaviour is comprised of three stages involving elasticity, where mean load is proportional to load range, an intermediate state where the effects of mean deflection cannot be ignored and a terminal state of significant plastic deformation which is affected by geometry changes and secondary membrane action.

Résumé

On étudie théoriquement et expérimentalement le comportement de poutres-consoles simples en acier doux soumises à des déflexions cycliques inégales en suivant la courbe moment-courbure de modèles appropriés, déterminés à partir de contrôles des déformations effectués sur des spécimens soumis à la flexion pure. Différents modèles sont proposés mettant en relation la courbure avec les limites des moments ainsi qu'avec le moment principal; les modèles s'adaptent aux phénomènes de durcissement et d'adoucissement d'un ensemble de fibres dans la section ainsi qu'à la relaxation du moment principal dans le temps. On montre que le comportement peut se diviser en trois étapes; une étape élastique où la charge principale est proportionnelle aux limites entre lesquelles varient les charges, une étape intermédiaire où les effets de la déflexion principale ne peuvent être ignorés et une étape finale de déformations plastiques importantes qui est perturbée par des changements dans la géométrie et des effets secondaires de membrane.

Zusammenfassung

Die Reaktion von Kragarmen aus normalem Baustahl auf zyklische nicht konstante Verformung wird theoretisch und experimentell untersucht, unter Ableitung von Angaben über dehnungskontrollierte Versuche an entsprechenden Momenten-Krümmungsmodellen bei reiner Biegung. Verschiedene Modelle werden vorgeschlagen, bei denen die Krümmung zum Momentenbereich und zum Mittelmoment in Zusammenhang gebracht wird. Die Modelle können Verfestigung und Abnahme der Festigkeit der Fasern der Querschnitte wie auch Relaxation infolge des Mittelmomentes beinhalten. Es wird gezeigt, dass das Verhalten drei Stadien umfasst: Elastizität, wobei das Mittelmoment proportional zum Lastbereich ist, ein Zwischenstadium, wobei die Effekte der Verformung nicht mehr vernachlässigt werden dürfen, und ein Endstadium mit signifikanten plastischen Deformationen, welche Änderungen der Geometrie und sekundäre Membranwirkung nach sich ziehen.